Biochimica et Biophysica Acta 1852 (2015) 490–506

Contents lists available at ScienceDirect

Biochimica et Biophysica Acta

journal homepage: www.elsevier.com/locate/bbadis

Muscle-specific GSK-3β ablation accelerates regeneration of disuse-atrophied skeletal muscle

Nicholas A.M. Pansters, Annemie M.W.J. Schols, Koen J.P. Verhees, Chiel C. de Theije, Frank J. Snepvangers, Marco C.J.M. Kelders, Niki D.J. Ubags, Astrid Haegens, Ramon C.J. Langen *

The Department of Respiratory Medicine, School for Nutrition and Translational Research in Metabolism (NUTRIM), Maastricht University Medical Centre (MUMC+), Maastricht, the Netherlands

ARTICLE INFO

Article history:
Received 2 May 2014
Received in revised form 26 November 2014
Accepted 3 December 2014
Available online 8 December 2014

Keywords:
Muscle regeneration
FoXO/atrogin/MuRF1
Akt/mTOR
Disuse-atrophy
MyoD/myogenin
Hindlimb suspension/reloading

ABSTRACT

Muscle wasting impairs physical performance, increases mortality and reduces medical intervention efficacy in chronic diseases and cancer. Developing proficient intervention strategies requires improved understanding of the molecular mechanisms governing muscle mass wasting and recovery. Involvement of muscle protein- and myonuclear turnover during recovery from muscle atrophy has received limited attention. The insulin-like growth factor (IGF)-I signaling pathway has been implicated in muscle mass regulation. As glycogen synthase kinase 3 (GSK-3) is inhibited by IGF-I signaling, we hypothesized that muscle-specific GSK-3β deletion facilitates the recovery of disuse-atrophied skeletal muscle. Wild-type mice and mice lacking muscle GSK-3β (MGSK-3β KO) were subjected to a hindlimb suspension model of reversible disuse-induced muscle atrophy and followed during recovery. Indices of muscle mass, protein synthesis and proteolysis, and post-natal myogenesis which contribute to myonuclear accretion, were monitored during the reloading of atrophied muscle. Early muscle mass recovery occurred more rapidly in MGSK-3β KO muscle. Reloading-associated changes in muscle protein turnover were not affected by GSK-3β ablation. However, coherent effects were observed in the extent and kinetics of satellite cell activation, proliferation and myogenic differentiation observed during reloading, suggestive of increased myonuclear accretion in regenerating skeletal muscle lacking GSK-3β. This study demonstrates that muscle mass recovery and post-natal myogenesis from disuse-atrophy are accelerated in the absence of GSK-3β.

1. Introduction

Chronic diseases, like congestive heart failure [1], rheumatoid arthritis [2,3], chronic renal failure, AIDS [4], chronic obstructive pulmonary disease (COPD) [5,6] and cancer [7,8] are associated with muscle wasting. Muscle wasting impairs physical performance, increases mortality and reduces efficacy of medical intervention [9]. Currently, muscle mass maintenance is an unmet-medical-need, which should be integrated in the management of chronic diseases and cancer. Developing proficient intervention strategies requires improved understanding of the molecular mechanisms governing muscle atrophy, hypertrophy, as well as muscle mass recovery-associated muscle regeneration. These mechanisms are regulated by balancing muscle protein synthesis and degradation, and potentially myonuclear loss and accretion, referred to as muscle protein-, and myonuclear turnover, respectively [10]. Involvement of these processes in muscle mass recovery following muscle atrophy has received limited attention.

Muscle protein synthesis can be initiated through insulin-like growth factor-I (IGF-I)-mediated activation of the Phosphatidylinositol-4,5-bisphosphate 3-kinase (PI-3K) signaling cascade leading to the phosphorylation of Akt/PKB at Thr308/Ser473 [11–13]. Activated Akt can subsequently phosphorylate both the mammalian target of rapamycin (mTOR)–raptor complex 1 (mTORC1) [14,15] and the two isoforms of GSK-3 [16,17], thereby initiating mRNA translation resulting in increased protein synthesis [18,19]. More specifically, activated mTOR, when phosphorylated at Ser2448, phosphorylates p70-S6K1 at Thr389 to stimulate translation capacity and hyper-phosphorylates eIF4E binding protein 1 (4E-BP1) to inhibit the suppression of translation initiation [15,20–22]. In addition, Akt phosphorylation of GSK-3β at Ser9 and GSK-3α at Ser21 suppresses GSK-3 function including its inhibitory phosphorylation of eIF2Bε at Ser540 [23,24], which allows eIF2Bε to interact with the eIF2-complex and facilitates mRNA translation initiation [25,26]. Muscle proteolysis involves several proteolytic systems, including the ubiquitin (Ub) 26S-proteasome system (UPS) and the autophagy–lysosomal pathway (ALP) [10,27,28]. The UPS entails selective proteolysis through the multi-ubiquitination of marked proteins by rate-limiting E3 ubiquitin ligases [29], which results in the degradation of the tagged proteins by the 26S-proteasome [30]. The E3 ligases muscle-specific atrogin-1/muscle atrophy F-box (MAFbx) (hereafter termed atrogin-1) and muscle-specific RING finger protein 1 (MuRF1) are upregulated under atrophic conditions [31,32] and regulate the proteolysis of myofibrillar proteins, muscle-specific enzymes

* Corresponding author at: Department of Respiratory Medicine, PO Box 5800, 6202 AZ Maastricht, the Netherlands. Tel.: +31 43 388 4247; fax: +31 43 387 5051.
E-mail address: r.langen@maastrichtuniversity.nl (R.C.J. Langen).

http://dx.doi.org/10.1016/j.bbadis.2014.12.006
0925-4439/

and transcription factors [33–36]. ALP-regulated autophagy clears long-lived proteins and dysfunctional organelles through autophagosome formation, which is initiated or aided by proteins like LC3, Gabarapl1 [37] and BNIP3 [38], whose presence is increased in atrophying muscle [37,39,40].

Quiescent satellite cells, located between the skeletal muscle basement and sarcolemmal membranes [41], are activated in response to muscle injury or exercise stimulation leading to muscle recovery [42–44]. The loss of myonuclei, and conversely activation and proliferation of satellite cells have been correlated to muscle atrophy and growth, respectively [45–49], implying a role for post-natal myogenesis and myonuclear accretion during muscle regeneration. Satellite cell activation results in increased PAX7 expression [50–52], and cell proliferation characterized by increased expression of Cyclin D1, PCNA or increased protein content of Ki-67 [53,54]. The resulting daughter myoblasts committed to muscle-specific differentiation fuse with existing myofibers [55], which are in part facilitated through cell–cell interaction sites containing muscle (M)-cadherin [56–58]. Myogenic differentiation includes muscle-specific gene expression regulated by muscle regulatory factors (MRFs), including Myf5, MyoD and Myogenin [59,60].

Altered expression of Mechano Growth Factor (MGF), a splice variant of IGF-I [61] accompanies local muscle repair, maintenance and remodeling [62,63]. Moreover, both muscle protein turnover and myonuclear turnover are subject to regulation by IGF-I signaling. Protein synthesis and muscle-specific gene expression can be stimulated by IGF-I [64–66], whereas muscle proteolysis is suppressed by IGF-I [14,67]. In addition, muscle-specific expression of IGF-I promotes muscle regeneration [68], and IGF-I signaling stimulates both the proliferative and differentiation potential of myoblasts [69–71]. Akt has been identified as a signaling molecule that coordinates IGF-I-mediated changes in muscle protein synthesis and degradation, but the regulation of myonuclear turnover by Akt is less well understood [72–74]. Ample evidence suggests an important role of the Akt substrate GSK-3 in muscle protein turnover, including muscle proteolysis during muscle atrophy [75–77], as well as myogenic differentiation and muscle regeneration [65,78,79]. Importantly, whereas GSK3α and GSK3β operate in a redundant manner in various cellular processes, previous studies suggest that muscle proteolysis and myogenic differentiation may be under unique control of GSK3β [75,79]. We therefore proposed a regulatory role of GSK-3β in skeletal muscle mass maintenance through its involvement in both protein and myonuclear turnover balances [17].

In the current study, we hypothesized that muscle-specific deletion of GSK-3β facilitates disuse-atrophied muscle mass recovery by stimulating signaling associated with net protein accretion and post-natal myogenesis. As inactivity is an important determinant of muscle atrophy associated with chronic disease and cancer [80], a model of reversible, hindlimb suspension (HS)-induced muscle atrophy was deployed to address this hypothesis. Wild-type Ctrl (WT) and muscle-specific (M)GSK-3β KO mice were subjected to HS and subsequent reloading (RL), and indices of muscle mass, protein synthesis, proteolysis signaling and myonuclear accretion were monitored during reloading-induced muscle mass recovery.

2. Materials and methods

2.1. Animals

The animal study described here was approved by the Institutional Animal Care Committee of Maastricht University (DEC-2009-074). Male skeletal muscle-specific (M)GSK-3β KO animals on a C57/Bl6 background were generated by breeding GSK-3$\beta^{fl/fl}$ MLC1f-Cre$^{+/-}$ (MGSK-3β KO) with GSK-3$\beta^{fl/fl}$ MLC1f-Cre$^{-/-}$ (Wild-type Ctrl/WT) mice [81]. Double Cre-negative litter mates served as 'wild type' (WT) controls. At the start of the experiment mice were 12.9 ± 1.1 weeks old (young adults) and weighed 27.7 ± 2.4 g. Animals were housed in a temperature controlled room (21–22 °C) with 12:12 h light–dark cycle, and received standard chow pellets and water ad libitum. Animals were randomly divided into 6 different groups for each genotype, and were subsequently subjected to no experimental procedures ('baseline'/RL-−14), 14 days of hindlimb suspension ('HS'/RL-0) or HS followed by 1, 2, 3, or 5 days of reloading (RL-1, -2, -3, -5, respectively). The group size was n = 8 except for MGSK-3β KO RL-5 (n = 7) and baseline for both genotypes (n = 9). A modified version of the HS/RL model [82] has previously been described [83]. In brief, a tail harness was placed while mice were lightly anesthetized using isoflurane inhalation. HS was accomplished using a tail suspension device consisting of a plastic-coated iron wire taped around the mouse's tail and connected to a swivel hook to allow circular motility. The latter was attached to a Teflon-coated PVC ring, which slid over an iron rod spanning the length of the cage to allow longitudinal motility. The mice were raised so as to prevent the hindlimbs from touching the cage floor or sides. In this way, four HS mice could be housed in one standard cage. After two weeks of HS, mice were again lightly anesthetized and released from the tail harness and allowed to resume normal cage activity. During the whole treatment period body weight and water consumption were monitored, in addition during the reloading phase chow consumption was assessed. After euthanasia with sodium pentobarbital at the indicated time points, lower leg muscles were excised using standardized dissection methods, cleaned of excess fat and tendon/connective tissue, pair weighed on an analytical balance, snap frozen in liquid nitrogen, and stored at −80 °C for RNA and protein extraction or part of the muscle was embedded in Tissue-Tek O.C.T. (Sakura, Finetek, Zoeterwoude, the Netherlands) for histological analyses. All subsequent analyses were performed in either soleus or gastrocnemius muscle, which despite their slightly differing anatomical positions and locomotive function, both respond to HS and RL alterations in muscle mass.

2.2. Western blot analysis

M. gastrocnemius was grounded into powder and homogenized in 400 μl of IP lysis buffer (50 mM Tris, 150 mM NaCl, 10% glycerol, 0.5% Nonidet P40, 1 mM EDTA, 1 mM Na_3VO_4, 5 mM NaF, 10 mM β-glycerophosphate, 1 mM $Na_4O_7P_2$, 1 mM dithiothreitol, 10 μg/ml leupeptin, 1% aprotenin, 1 mM PMSF, pH 7.4) with a Polytron PT 1600 E (Kinematica). After homogenization, the samples were incubated for 15 min on a rotating wheel at 4 °C and spun for 30 min at maximum speed (20,817 ×g) in a centrifuge cooled to 4 °C. The supernatant was aliquoted, snap-frozen, and stored without sample buffer at −80 °C until analysis. A portion of the supernatant was saved for protein determination, prior to the addition with 4× Laemmli sample buffer (0.25 M Tris–HCl pH 6.8; 8% (w/v) SDS; 40% (v/v) glycerol; 0.4 M DTT and 0.04% (w/v) Bromophenol Blue). The samples were boiled for 5 min at 95 °C and stored at −80 °C. Total protein was assessed by the Thermo Scientific Pierce BCA Protein Assay kit (Pierce Biotechnology, IL, USA) according to the manufacturer's instructions. The pellet fraction was re-suspended in IP lysis buffer and homogenized with a Polytron PT 1600 E (Kinematica), subsequently 4× Laemmli sample buffer was added and boiled for 5 min at 95 °C and stored at −80 °C. For SDS-PAGE 0.2 μg–15 μg of protein was loaded per lane and separated on a Criterion™ XT Precast 4–12% Bis-Tris gel (Bio-Rad, #3450124), followed by transfer to a 0.45 μm Whatman® Protran® Nitrocellulose Transfer membrane (Whatman GmbH, #7324007) by electroblotting (Bio-Rad Criterion Blotter) (Bio-Rad, Hercules, CA, USA). For the pellet fraction containing protein loaded samples the membrane was stained with Ponceau S solution (0.2% Ponceau S in 1% acetic acid; Sigma-Aldrich Chemie) to quantify total protein loading. The membrane was blocked for 1–2 h at room temperature in 5% (w/v) NFDM (non-fat dried milk) (ELK, Campina, the Netherlands) diluted in TBS-Tween-20 (0.05%). Nitrocellulose blots were washed in TBS-Tween-20 (0.05%) on a rotating platform, followed by overnight (o/n) incubation at 4 °C with specific antibodies directed against: p-mTOR (Ser2448) (#2971), mTOR (#2983), p-Akt (Ser473) (#9271), Akt (#9272), p-GSK-3β

(Ser9) (#9336), GSK-3β (#9332), p-p70S6K (Thr389) (#9206), p70S6K (#2708), 4E-BP1 (#9452), p-FoXO1 (Ser256) (#9461), FoXO1 (#2880), p-FoXO1/3a (Thr24) (#9946), and GAPDH (#2118) (all from Cell Signaling Technology, Inc., Danvers, MA), myosin heavy chain fast (MyHC-f/MHC-2) (#M4276, Sigma-Aldrich) all diluted in TBS/0.05% Tween-20 with or without 5% BSA/NFDM. After 3 washing steps of 10 min each, the blots were probed with a peroxidase conjugated secondary antibody (Vector Laboratories, #PI-1000), and visualized by chemiluminescence using Supersignal® WestPico Chemiluminescent Substrate (Pierce Biotechnology, Inc.) according to the manufacturers' instructions and exposed to film (Biomax light film, KODAK) or live imaged (Bio-Rad chemidoc XRS). Western blot images were quantified using the Quantity One analysis software from Bio-Rad. For analyses, gels were loaded with both WT and MGSK-3β KO samples, and samples of the same group were distributed over multiple gels to allow comparisons to RL-0 (HS).

2.3. RNA isolation and assessment of mRNA abundance by RT-qPCR

M. gastrocnemius was grounded into powder and approximately 10 mg of sample was suspended and lysed in RLT solution containing 1% β-mercaptoethanol. Samples were further processed according to manufacturer's instructions of the RNeasy fibrous tissue Mini Kit (Qiagen, Venlo, the Netherlands) including the on-column DNase treatment. RNA was reconstituted in 50 μl RNase free water and stored at −80 °C. The RNA concentrations were measured spectrophotometrically using a Nanodrop® ND-1000 UV–Vis spectrophotometer. RNA was diluted >5× in ddH_2O and 400 ng of RNA was reverse transcribed to cDNA using the Transcriptor first strand cDNA synthesis kit (Roche Diagnostics GmbH, Mannheim, Germany) with anchored oligo-dT primers according to the manufacturer's conditions for generating cDNA fragment of 4 kb in a final reaction volume of 20 μl. This cDNA was used for the quantification of transcript levels by reverse transcription quantitative PCR (qPCR) analysis. qPCR primers used, were designed using Primer Express 2.0 software (Applied Biosystems, Foster City, CA), and obtained from Sigma Genosys (Haverhill, UK). qPCR reactions (16 μl final volume) contained SensiMix SYBR Hi-ROX Kit (Quantace-Bioline, London, UK) with 300 nM primers and were run in a 384-well MicroAmp Optical 384-Well Reaction Plate (Applied Biosystems, Nieuwerkerk a/d IJssel, the Netherlands) on a 7900HT Fast Real-Time PCR System (Applied Biosystems). Relative cDNA starting quantities for the samples were derived by the standard curve method. Standard curve samples were generated by serial dilution of pooled cDNA samples. Starting quantities were obtained by extrapolating Ct values on the standard curve. The expression of the genes of interest was normalized with a correction factor derived by GeNorm [84]. This factor was determined for each group individually to reduce variation in data resulting from biological spread and analytical imperfections, as reference gene expression between time points responded significantly, in line with observations by others [85]. The GeNorm correction factor was based on the expression levels of GAPDH, RPL13A, ARBP, Calnexin and β2M as reference genes.

2.4. Immunohistochemical analyses

Histological analysis of cell proliferation and myofiber cross sectional area was performed on M. soleus, as fiber type composition and CSA are less heterogeneous compared to M. gastrocnemius [86]. Furthermore compared to the gastrocnemius, the soleus muscle has greater load-sensitivity and thus greater morphological remodeling processes are expected to be undertaken during the reloading phase [87]. OCT-embedded, frozen M. soleus sections were cut (5 μm), air dried, treated with 0.5% Triton X-100 in PBS, incubated with primary anti-myosin heavy chain (MyHC)-I [Developmental Studies Hybridoma Bank (DSHB), University of Iowa, Ames, IA], anti-MyHC-IIa (DSHB), and anti-laminin (Sigma, Zwijndrecht, the Netherlands) followed by secondary antibodies labeled with Alexa Fluor 555, Alexa Fluor 488, and Alexa Fluor 350 (Invitrogen, Breda, the Netherlands). Unstained fibers were considered type IIX/B fibers. After staining, all images were digitally captured using fluorescence microscopy (Nikon Instruments Europe). Image processing and quantitative analyses were done using the Lucia 4.81 software package. The mean fiber CSA of each muscle was calculated by analyzing on average >200 fibers per muscle. Additionally frozen M. soleus sections were cut (5 μm), were air dried, treated with 0.5% Triton X-100 in PBS, and incubated with primary anti-laminin (Sigma, Zwijndrecht, the Netherlands) and Ki-67 (Biocare medical/klinipath,Pigeons, the Netherlands) followed by secondary antibodies labeled with Alexa Fluor 488, and Alexa Fluor 350 (Invitrogen, Breda, the Netherlands) and propidium iodide (PI) for nuclear staining. After staining, all images were digitally captured using fluorescence microscopy (Nikon Instruments Europe). Image processing and quantitative analyses were done using the Lucia 4.81 software package. Double stained (PI and Ki-67) nuclei were counted as proliferating nuclei and divided by the number of fibers per muscle section analyzed to determine the proliferation level for that specific muscle.

2.5. Statistical analysis

Statistical data analysis was performed ($n = 4–9$) to allow comparisons between Wild-type littermate Ctrl (WT) vs. MGSK-3β KO mice at specific time points, and within genotypes between a specific time point vs. RL-0 (HS). Significant differences were detected with a non-parametric Mann–Whitney U test, $p < 0.05$ or smaller as indicated in each figure. Data are expressed as mean ± SEM. Data were analyzed using SPSS/PC+ (Statistical Package for the Social Sciences, Version 22.0 for Windows; SPSS; Chicago, IL).

3. Results

3.1. Muscle specific deletion of GSK-3β accelerates bodyweight recovery and muscle MGF expression during muscle reloading

GSK-3β protein content was reduced (~95%) in M. gastrocnemius of MGSK-3β KO compared to WT mice (Fig. 1A), whereas GSK-3α protein levels were unaffected. This allowed us to address GSK3β functions that are either non-redundant with GSK-3α, or are dependent on total GSK3 levels. eIF2Bε (Ser539) phosphorylation, a downstream target of GSK-3 enzymatic activity [88], was significantly lower in MGSK-3β KO muscle ($p < 0.05$) (Fig. 2D). Hindlimb suspension (HS) resulted in approximately 10% bodyweight (BW) loss (Fig. 1B, left panel). The genotypic difference ($p < 0.05$) in the initial BW loss after two days of HS (Fig. 1B, left panel) suggested a short term (initial 24–72 h of HS) protective effect in MGSK-3β KO mice compared to Wild-type Ctrl (WT) mice. During the five day reloading (RL) period BW significantly increased ($p < 0.001$) compared to HS (RL-0) for both genotypes (Fig. 1B, right panel). However, compared to WT, BW recovery following five days of RL was significantly greater in MGSK-3β KO mice (6.7 ± 1.2% v.s. 11.3 ± 0.8%, $p < 0.05$). Fourteen days of HS comparably decreased muscle mass in both WT and MGSK-3β KO mice (16.9 ± 2.7%, $p < 0.001$ and 16.3 ± 2.2%, $p < 0.001$, respectively, Fig. 1C, left panel). Importantly, alterations in unloading-sensitive muscle mass were attributable to unloading, as no changes in the unloading-insensitive M. extensor digitorum longus (EDL) were observed (data not shown). Subsequent hindlimb RL showed a comparable but not statistical significant increase in gastrocnemius muscle mass for WT and MGSK-3β KO (6.6 ± 2.6% and 5.8 ± 4.6%, Fig. 1C, right panel). Accordingly, the evaluation of myofibrillar protein accretion revealed increases in MHC-2 (glycolytic isoform) content in M. gastrocnemius homogenates following 5 days RL (38.7 ± 7.6%, $p < 0.01$ and 27.8 ± 5.6%, $p < 0.01$, Fig. 1D, right panel), in line with net muscle tissue accretion. Expression of Mechano Growth Factor (MGF), produced during muscle remodeling [89], was clearly induced

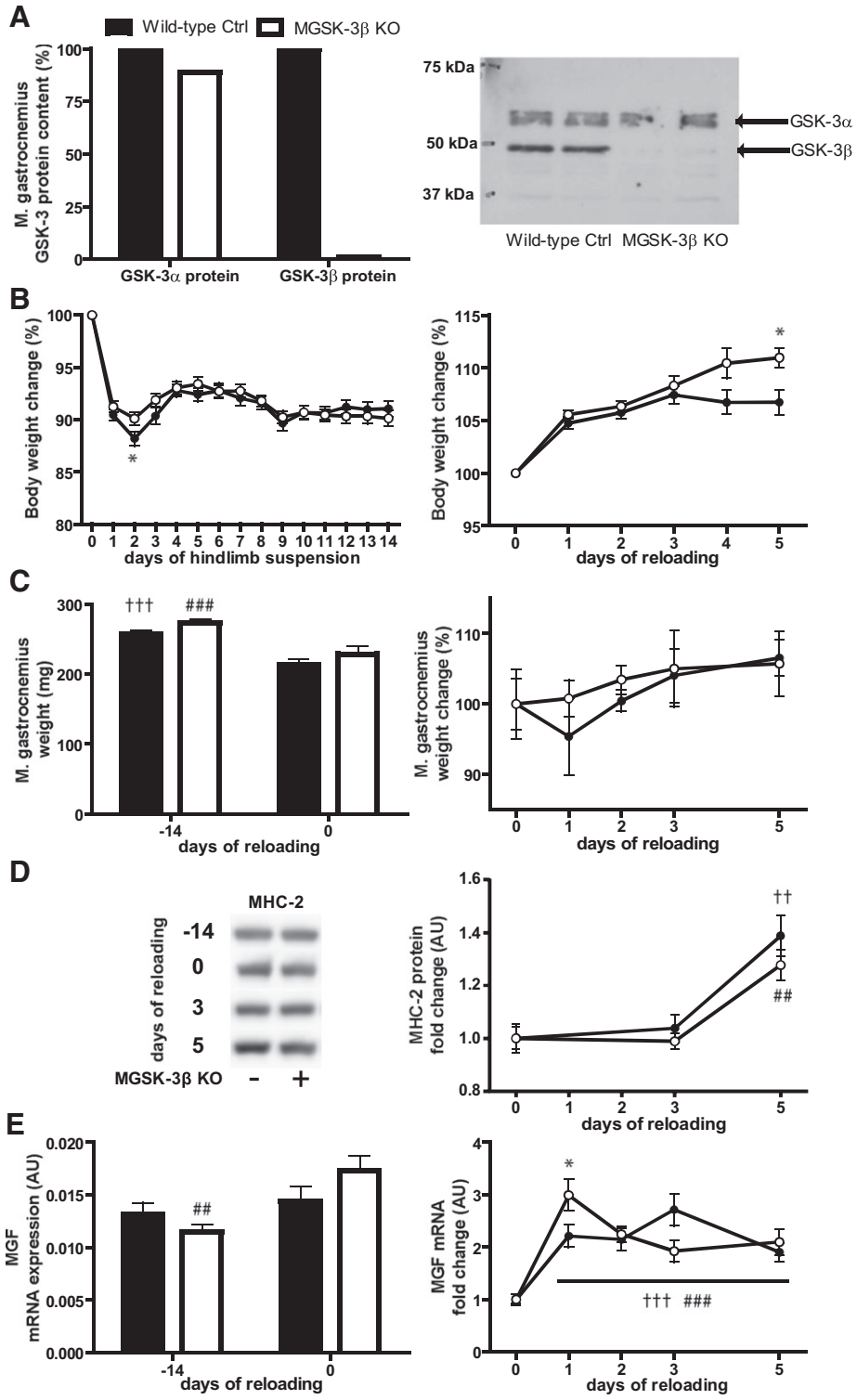

Fig. 1. Muscle specific deletion of GSK-3β accelerates bodyweight recovery and muscle MGF expression during muscle reloading. (A) M. gastrocnemius protein lysates were subjected to Western blot and GSK-3β knockdown levels and GSK-3α expression levels were assessed (WT/MGSK-3β KO n = 2). Muscle-specific GSK-3β KO or littermate controls (WT) were subjected to 14 days of hindlimb suspension (HS). (B) Bodyweight (BW) was monitored and expressed as percentage change of starting bodyweight during HS (left panel, WT n = 40, MGSK-3β KO n = 39). Following the completion of HS and during reloading (RL) BW, expressed as percentage change of BW at the start of RL (RL-0/HS; right panel, both WT/KO decrease with n = 8 increments). (C) Paired gastrocnemius muscle weights were determined at baseline ('RL-−14') and after HS ('RL-0'; left panel). Alternatively, during RL M. gastrocnemius weights were expressed as percentage of HS (RL-0) muscle weight (right panel). (D) Glycolytic myosin heavy chain (MHC-2) protein contents were detected in re-solubilized muscle homogenate pellet fraction, normalized to total protein determined by Ponceau-S staining, and expressed as fold change of HS (RL-0). (E) Mechano Growth Factor (MGF) mRNA levels were determined during baseline and following HS (left panel), or during RL (right panel). MGF expression levels during RL are presented as fold change compared to RL-0 (HS) to illustrate reloading-induced changes. (C–E group size was n = 8 except for MGSK-3β KO RL-5 n = 7 and baseline for both genotypes n = 9). Averages ± SEM are presented, *: Wild-type Ctrl vs. MGSK-3β KO at that specific time point, †: indicates time effect compared to RL-0 (HS) for Wild-type Ctrl and #: indicates time effect compared to RL-0 (HS) for MGSK-3β KO; 1 symbol equals $p < 0.05$, 2 symbols equal $p < 0.01$, and 3 symbols equal $p < 0.001$.

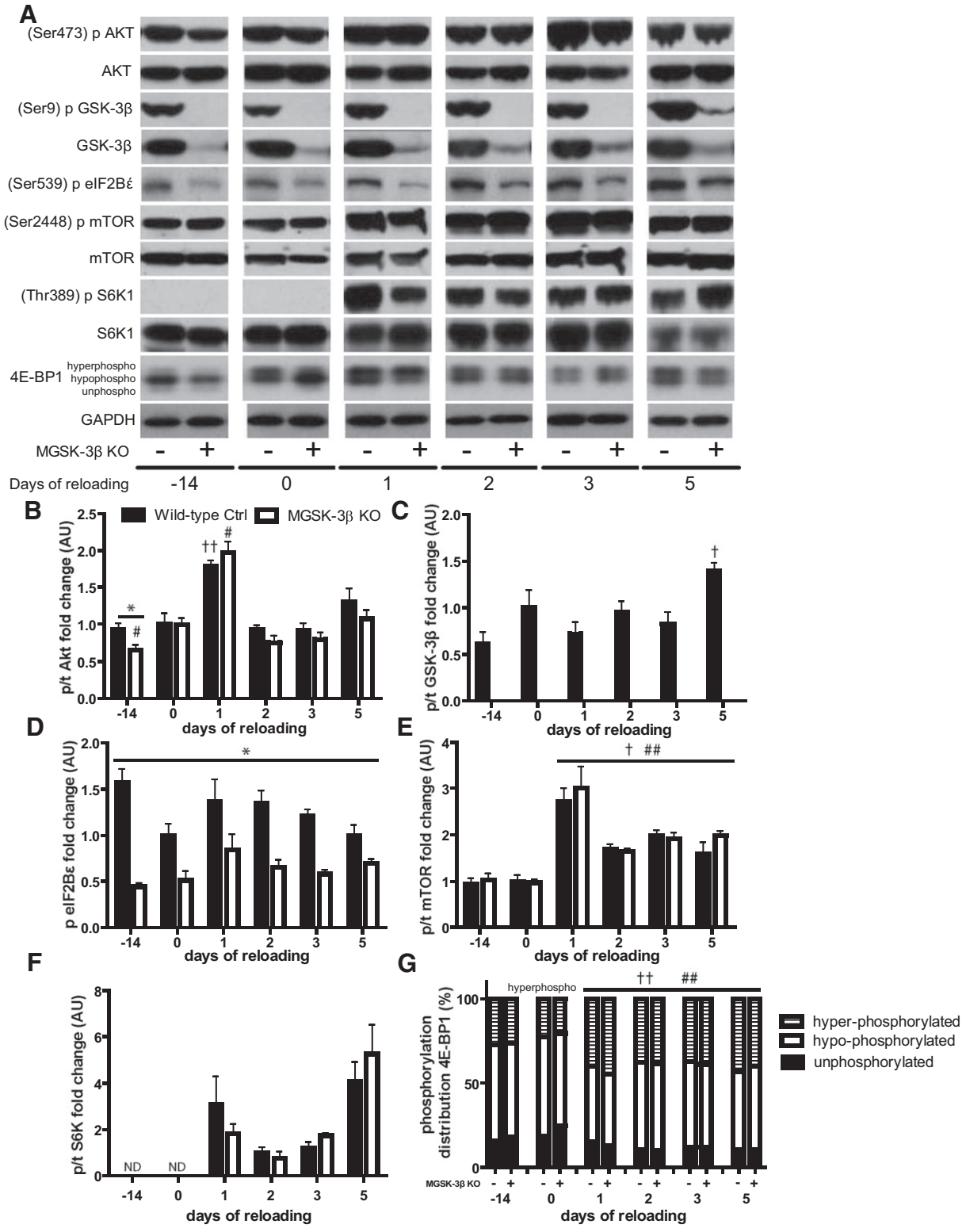

Fig. 2. Activation of Akt–mTOR signaling during muscle reloading is not affected by the absence of GSK-3β. (A) M. gastrocnemius was prepared for Western blot analysis and indicated phosphorylated and total proteins were detected to determine protein synthesis signaling status. Subsequently, (B) Akt phosphorylation, (C) GSK-3β phosphorylation, (D) eIF2Bε phosphorylation, (E) mTOR phosphorylation. (F) p70-S6K1 phosphorylation and (G) 4E-BP1 phosphorylated-isoform distribution were quantitatively assessed. (B–G group size was n = 6–9 for both WT and MGSK-3β KO). Averages ± SEM are presented, *: Wild-type Ctrl vs. MGSK-3β KO at that specific time point, †: indicates time effect compared to RL-0 (HS) for Wild-type Ctrl and #: indicates time effect compared to RL-0 (HS) for MGSK-3β KO; 1 symbol equals $p < 0.05$, 2 symbols equal $p < 0.01$, and 3 symbols equal $p < 0.001$.

on RL day 1 (RL-1), suggesting the initiation of muscle regeneration in both WT and MGSK-3β KO M. gastrocnemius (Fig. 1E, right panel). Although MGF expression levels were not significantly different between genotypes at baseline (RL-— 14) or after HS (RL-0) in Fig. 1E (left panel), HS increased MGF expression compared to baseline levels in MGSK-3β KO but not WT (50.9 ± 4.1%, $p < 0.01$ vs. 9.39 ± 7.6% n.s.). During RL, MGF expression was up-regulated (~two-fold, $p < 0.01$) in both WT and MGSK-3β KO (Fig. 1E, right panel). However, MGF expression

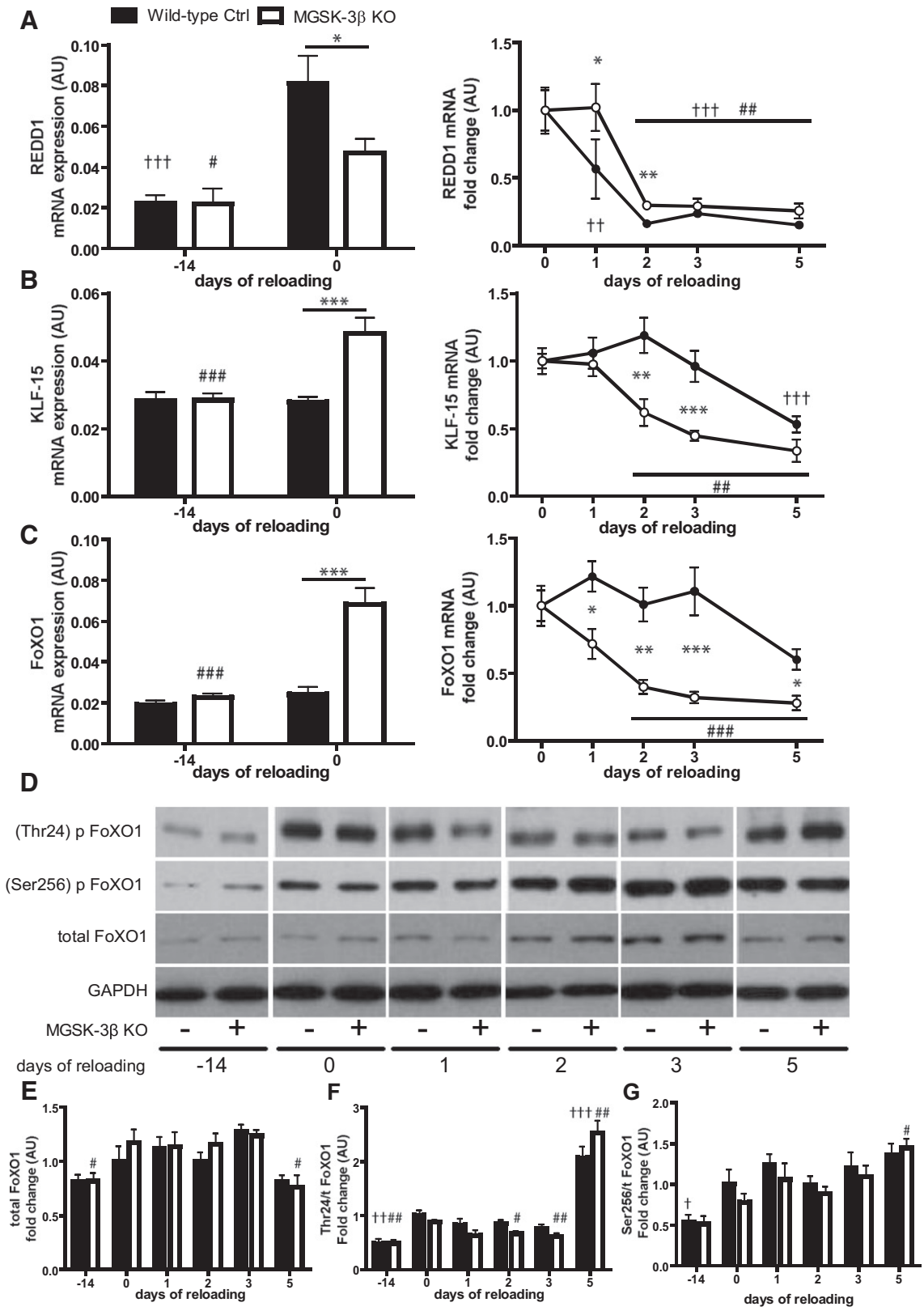

Fig. 3. Differential effects of GSK-3β deletion on changes in the expression of glucocorticoid sensitive regulators of protein turnover signaling during muscle unloading and reloading. M. gastrocnemius was prepared for gene expression analysis and (A) REDD1 (B) KLF-15 and (C) FoXO1 were detected to determine protein degradation signaling status after HS and fold change compared to start reloading (RL-0/HS) gene expression levels during RL (A–C group size was n = 7–9 for both WT and MGSK-3β KO). (D) M. gastrocnemius was prepared for Western blot analysis and indicated total (E) FoXO1, (F) Thr24 and (G) Ser256 FoXO1 phosphorylation were quantitatively assessed to determine protein degradation signaling status. (D–G group size was n = 7–8 except for MGSK-3β KO RL-0 n = 4 and baseline for both genotypes n = 9). Averages ± SEM are presented, *: Wild-type Ctrl vs. MGSK-3β KO at that specific time point, †: indicates time effect compared to RL-0 (HS) for Wild-type Ctrl and #: indicates time effect compared to RL-0 (HS) for MGSK-3β KO; 1 symbol equals $p < 0.05$, 2 symbols equal $p < 0.01$, and 3 symbols equal $p < 0.001$.

induction on RL-1 was more pronounced ($p < 0.05$) in MGSK-3β KO compared to WT (3.0 ± 0.3-fold, $p < 0.001$ vs. 2.2 ± 0.2-fold, $p < 0.001$, Fig. 1E, right graph). Combined, these data indicate that reloading-induced muscle remodeling may be affected by GSK-3β.

3.2. Activation of Akt–mTOR signaling during muscle reloading is not affected by the absence of GSK-3β

Hindlimb reloading initiates the muscle remodeling process which involves adjusting the protein turnover balance regulated by protein synthesis and degradation signaling [78,90–92]. Akt (Ser473) phosphorylation is lower in MGSK-3β KO compared to WT at baseline (RL-−14) ($p < 0.05$, Fig. 2B). Akt-phosphorylation levels were not affected by HS (RL-0) in WT but were increased in MGSK-3β KO (3.6 ± 15.7% vs. 49.8 ± 13.6%, $p < 0.05$, Fig. 2B), and thereby no longer genotypically different from WT. At RL-1 Akt-phosphorylation increased, compared to HS (RL-0), for WT and MSGK-3β KO (77.8 ± 8.8%, $p < 0.01$ and 97.0 ± 15.1%, $p < 0.05$, respectively, Fig. 2B). During further RL days, Akt phosphorylation decreased again to HS comparable levels for both genotypes. After HS downstream from Akt, inactivating GSK-3β (Ser9) phosphorylation was increased by ~50% in WT (Fig. 2C). Following HS, GSK-3β phosphorylation did not significantly increase until RL-5 (39.2 ± 8.9%, $p < 0.05$, Fig. 3C). This coincided with a similar increase in WT Akt phosphorylation (30.5 ± 18.1%, Fig. 2B) at RL-5. As expected, eIF2Bε (Ser539) phosphorylation, downstream target of GSK-3β phosphorylation [88], was significantly lower in MGSK-3β KO ($p < 0.05$) and did not alter throughout HS–RL (Fig. 2D). Although in WT muscle eIF2Bε phosphorylation did not significantly change during HS-RL, phospho levels appeared to inversely reflect GSK-3β phosphorylation changes at RL-0 and RL-5 (Fig. 2D and C).

mTOR (Ser2448) phosphorylation levels were unaltered after HS and not different between genotypes (Fig. 2E). However, mTOR phosphorylation increased as of RL-1 in both WT and MGSK-3β KO muscles (2.7 ± 0.3-fold, $p < 0.01$, and 3.1 ± 0.5-fold, $p < 0.001$, no genotypic difference), leveling off above HS levels at RL-2 and later time points (>1.5-fold, $p < 0.05$), with no genotypic effect of GSK-3β ablation (Fig. 2E). S6K (Thr389) phosphorylation, a major downstream target of mTOR and effector of mRNA translation capacity, was not detectable at either baseline (RL-−14) or after HS (RL-0) for either genotype (Fig. 2F). However, the initiation of RL clearly increased S6K phosphorylation (Fig. 2F). Following the initial increase on RL-1, S6K phosphorylation decreased on RL-2 and RL-3, while it increased again at RL-5 for both WT and MGSK-3β KO (1.3 ± 0.3 AU and 2.9 ± 0.7 AU, respectively, Fig. 2F) with no statistically significant genotypic effects throughout RL. This biphasic response was not observed in mTOR phosphorylation changes (Fig. 2C), but was apparent in Akt phosphorylation changes (Fig. 2B). Phosphorylation levels of the suppressor of mRNA translation initiation 4E-BP1 were, in line with S6K and mTOR, unchanged after HS (Fig. 2G). However, RL initiation increased 4E-BP1 phosphorylation evidenced by a shift from the relative proportion of un-phosphorylated to hyper-phosphorylated (inactivating) 4E-BP1. Hyper-phosphorylation of 4E-BP1 increased for both WT and MSGK-3β KO (42.2 ± 0.7%, $p < 0.01$ and 76.8 ± 10.9%, $p < 0.01$, respectively) on RL-1 and remained elevated subsequently till RL-5 for both genotypes (>30%, $p < 0.01$, Fig. 2G). The inverse was observed for un-phosphorylated 4E-BP1; with no observed effect of GSK-3β ablation on 4E-BP1 phosphorylation distribution during HS–RL (Fig. 2G). Thus, apart from its direct target eIF2Bε, the deletion of GSK-3β does not appear to affect increased protein synthesis signaling in atrophied muscle in response to RL.

3.3. Differential effects of GSK-3β deletion on changes in the expression of glucocorticoid sensitive regulators of protein turnover signaling during muscle unloading and reloading

Skeletal muscle protein turnover is affected by glucocorticoid (GC) receptor (GR) signaling [39,93–96]. GR-mediated transcription of REDD1 has been implicated in the inhibition of protein synthesis [20,97]. HS was accompanied by an up-regulation of REDD1 expression in WT and MGSK-3β KO (3.6 ± 0.6-fold, $p < 0.001$ and 2.1 ± 0.3-fold, $p < 0.05$, respectively), which was most pronounced in WT muscle (1.7-fold higher than in MGSK-3β KO, $p < 0.05$; Fig. 3A, left panel). The subsequent decrease in REDD1 expression after RL-1 observed in WT (1.8-fold, $p < 0.01$) was absent in MGSK-3β KO (Fig. 3A, right panel). From RL-2 onwards, both WT ($p < 0.001$) and MGSK-3β KO ($p < 0.01$) displayed >70% decrease in REDD1 mRNA expression compared to RL-0 (Fig. 3A, right panel).

KLF-15 [98,99], and FoXO1 [98,100] are two transcriptional regulators of proteolysis affected by the GR. KLF-15 was not altered after HS in WT, but increased in MGSK-3β KO (1.0 ± 0.1-fold vs. 1.7 ± 0.2-fold, $p < 0.001$, respectively; Fig. 3B, left panel), with levels differing between WT and MGSK-3β KO (1.7-fold, $p < 0.001$; Fig. 3B, left panel). Initiation of RL decreased KLF15 expression until RL-5 for both WT and MGSK-3β KO (46.7 ± 5.8%, $p < 0.001$ and 66.3 ± 8.3%, $p < 0.01$, respectively), but this decrease started already at RL-2 in MGSK-3β KO muscle (1.6 ± 0.1-fold, $p < 0.01$) and was more pronounced compared to WT (RL-2 and RL-3, $p < 0.01$; Fig. 3B, right panel). Interestingly FoXO1 expression changes throughout HS–RL were relatively similar to KLF15 expression changes (Fig. 3C and B, respectively). FoXO1 total protein content was increased after HS for both WT and MGSK-3β KO (1.2 ± 0.1-fold and 1.4 ± 0.1, $p < 0.05$, respectively; Fig. 3D–E) and remained relatively unchanged until RL-5, when it decreased to RL- −14 (BL) comparable levels (1.2 ± 0.1-fold and 1.5 ± 0.1, $p < 0.05$, respectively; Fig. 3E). FoXO activity is strongly regulated by its phosphorylation status, which facilitates its nuclear exclusion [101]. HS resulted in increased phosphorylation of FoXO1, which was more pronounced in WT (Thr24 and Ser256, 2.1 ± 0.2-fold and 1.9 ± 0.3-fold, respectively, $p < 0.05$) compared to MGSK-3β KO (Thr24 and Ser256, 1.8 ± 0.1-fold, $p < 0.01$ and 1.5 ± 0.2-fold, respectively; Fig. 3F and G). During RL FoXO1 Thr24 phosphorylation appeared to decrease for both genotypes, but only significantly in MGSK-3β KO (>25% RL-2 and RL-3, $p < 0.05$; Fig. 3F). In contrast, at RL-5 FoXO1 phosphorylation strongly increased compared to RL-0 for both WT (Thr24 and Ser256, 2.1 ± 0.2-fold, $p < 0.001$ and 1.4 ± 0.1-fold, respectively) and MGSK-3β KO (Thr24 and Ser256, 2.9 ± 0.3-fold, $p < 0.01$ and 1.8 ± 0.1-fold, $p < 0.05$, respectively; Fig. 3F–G). Considering the extensive regulation of FoXO during HS and RL in both genotypes, FoXO transcriptional targets involved in muscle protein degradation were subsequently investigated.

3.4. Expression of proteolysis mediators is decreased during muscle reloading and differentially affected by the absence of GSK-3β

Atrogin-1 gene expression was lower at baseline (RL-−14) in MGSK-3β KO than WT (~1.5-fold, $p < 0.01$), and increased similarly following HS in both WT and MGSK-3β KO (1.5 ± 0.2-fold, $p < 0.05$ and 1.6 ± 0.2-fold, respectively), sustaining the genotypic difference ($p < 0.05$; Fig. 4A, left panel). With RL, atrogin-1 gene expression levels decreased similarly for WT and MGSK-3β KO till RL-5 (>3.5-fold, $p < 0.01$; Fig. 4A, right panel). Contrary to atrogin-1, MuRF1 gene expression was not different between genotypes at baseline, nor significantly induced after HS in either WT or MGSK-3β KO (Fig. 4B, left graph). RL-associated MuRF1 gene expression suppression (>2.5-fold, $p < 0.05$; Fig. 4B, right panel) occurred more rapidly in MGSK 3β KO, similar to REDD1 and FoXO1 (Fig. 3A and C, right panels). Interestingly, MuRF1 expression transiently increased in both WT and MGSK-3β KO muscles at RL-3 (1.4 ± 0.1-fold and 1.8 ± 0.2-fold compared to RL-2, respectively; Fig. 4B, right panel), corresponding with the biphasic response of FoXO1 phosphorylation (Fig. 3F–G). Autophagy mediator BNIP3 baseline mRNA levels were unaffected by muscle-specific GSK-3β ablation (Fig. 4C, left panel). Although HS increased BNIP3 expression in both WT and MGSK-3β KO (13.6 ± 5.7%, $p < 0.05$ and 64.8 ± 8.8%, $p < 0.001$, respectively), it resulted in a significantly different genotypic response ($p < 0.001$; Fig. 4C, left panel). BNIP3 expression

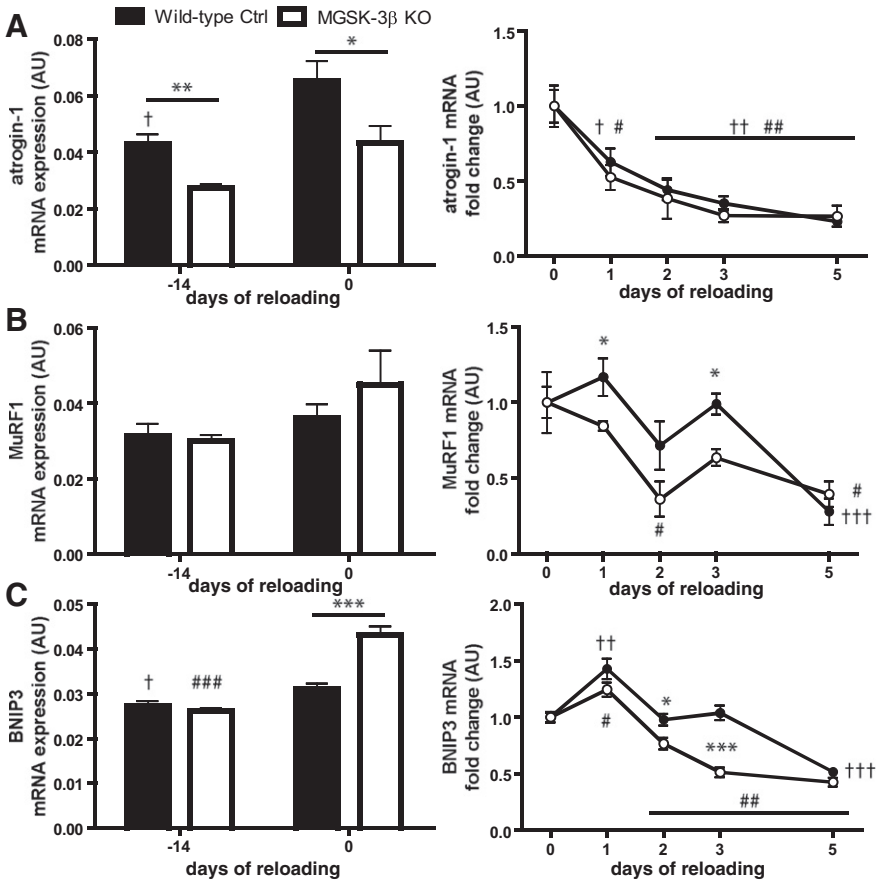

Fig. 4. Expression of proteolysis mediators is decreased during muscle reloading and differentially affected by the absence of GSK-3β. M. gastrocnemius was prepared for gene expression analysis and (A) atrogin-1, (B) MuRF1 and (C) BNIP3 were detected to determine possible effects of protein degradation signaling status after FoXO1 phosphorylation changes due to HS and fold change compared to start reloading (RL-0) gene expression levels during RL. (A–C group size was n = 7–9 for both WT and MGSK-3β KO). Averages ± SEM are presented, *: Wild-type Ctrl vs. MGSK-3β KO at that specific time point, †: indicates time effect compared to RL-0 (HS) for Wild-type Ctrl and #: indicates time effect compared to RL-0 (HS) for MGSK-3β KO; 1 symbol equals $p < 0.05$, 2 symbols equal $p < 0.01$, and 3 symbols equal $p < 0.001$.

transiently increased during the initial RL for WT and MGSK-3β KO (RL-1: 1.4 ± 0.1-fold, $p < 0.01$ and 1.2 ± 0.1-fold, respectively), but subsequently decreased until RL-5 for both genotypes (>1.9-fold, $p < 0.001$). However, BNIP3 expression decreased more rapidly in MGSK-3β KO compared to WT on RL-2 and RL-3 ($p < 0.05$ and $p < 0.001$, respectively; Fig. 4C, right panel).

3.5. Rapid induction of cell proliferation upon muscle reloading is not affected by GSK-3β ablation

To assess whether HS–RL induced muscle remodeling involves satellite cell proliferative responses which are affected by muscle-specific GSK-3β ablation, Cyclin D1 and PCNA gene expression levels were determined in the gastrocnemius muscle. Although at baseline (RL-−14) Cyclin D1 expression was ~1.5-fold ($p < 0.05$) lower in MGSK-3β KO compared to WT, HS decreased Cyclin D1 expression for both WT and MGSK-3β KO to comparable levels (2.2 ± 0.2-fold; $p < 0.001$ and 1.4 ± 0.1-fold, respectively; Fig. 5A, left panel). Cyclin D1 levels rapidly increased with RL in both WT and MGSK-3β KO (RL-1: 4.3 ± 0.7-fold, $p < 0.001$ and 5.0 ± 0.2-fold, $p < 0.001$, respectively; Fig. 5A, right panel), and remained elevated throughout RL for both genotypes (~2.5-fold, $p < 0.01$; Fig. 5A, right panel). PCNA baseline expression was not significantly altered by HS or genotypically different (Fig. 5B, left panel). Similar to Cyclin D1, PCNA gene expression rapidly increased with RL in both WT and MGSK-3β KO (RL-1: 3.5 ± 0.5-fold, $p < 0.05$ and 3.1 ± 0.6-fold, $p < 0.05$, respectively; Fig. 5B, right panel), and displayed a biphasic response. In contrast to Cyclin D1, both WT and MGSK-3β KO PCNA expression levels had returned to RL-0 (HS) comparable levels at RL-5 (Fig. 5B, right panel). A Ki-67 protein staining was used to visualize cell proliferation in the soleus muscle using immunohistochemistry (Fig. 5C). Very few positive nuclei were observed at baseline (RL-−14), or directly following HS (RL-0). In contrast, striking increases in cellular Ki-67 staining appeared on RL-3 and RL-5 (>18-fold; Fig. 5D), indicating active cell proliferation in the soleus muscle. However, GSK-3β ablation did not significantly affect the number of proliferating cells.

3.6. Absence of GSK-3β enhances myogenesis-associated gene expression upon muscle reloading

To assess whether the increase in cell proliferation was accompanied by a myogenic regenerative response, satellite cell activation and myogenesis were probed. PAX-7 expression was not changed after HS for both WT and MGSK-3β KO (Fig. 6A, left panel). Similar to Cyclin D1 and PCNA, PAX-7 transcript levels strongly increased on RL-1 in both WT and MGSK-3β KO (1.6 ± 0.3-fold and 1.9 ± 0.3-fold, $p < 0.01$, respectively), and decreased at RL-5 (1.5 ± 0.1-fold and 1.9 ± 0.1-fold, $p < 0.01$, respectively; Fig. 6A, right panel) to levels below RL-0 (HS). However, only in WT, PAX7 expression levels progressed with a biphasic response throughout RL (WT vs. MGSK-3β KO ~2.5-fold, $p < 0.01$ on RL-3; Fig. 6A right panel), similar to patterns of Cyclin D1 and PCNA expression. M-cadherin transcript levels were elevated in response to HS only in MGSK-3β KO, resulting in a difference between WT and GSK3-KO following HS (RL-0: 1.2 ± 0.1-fold and 1.7 ± 0.1-fold, $p < 0.001$, respectively; Fig. 6B, left panel). RL induced M-cadherin expression changes progressed very similar to PAX7 (Fig. 6A

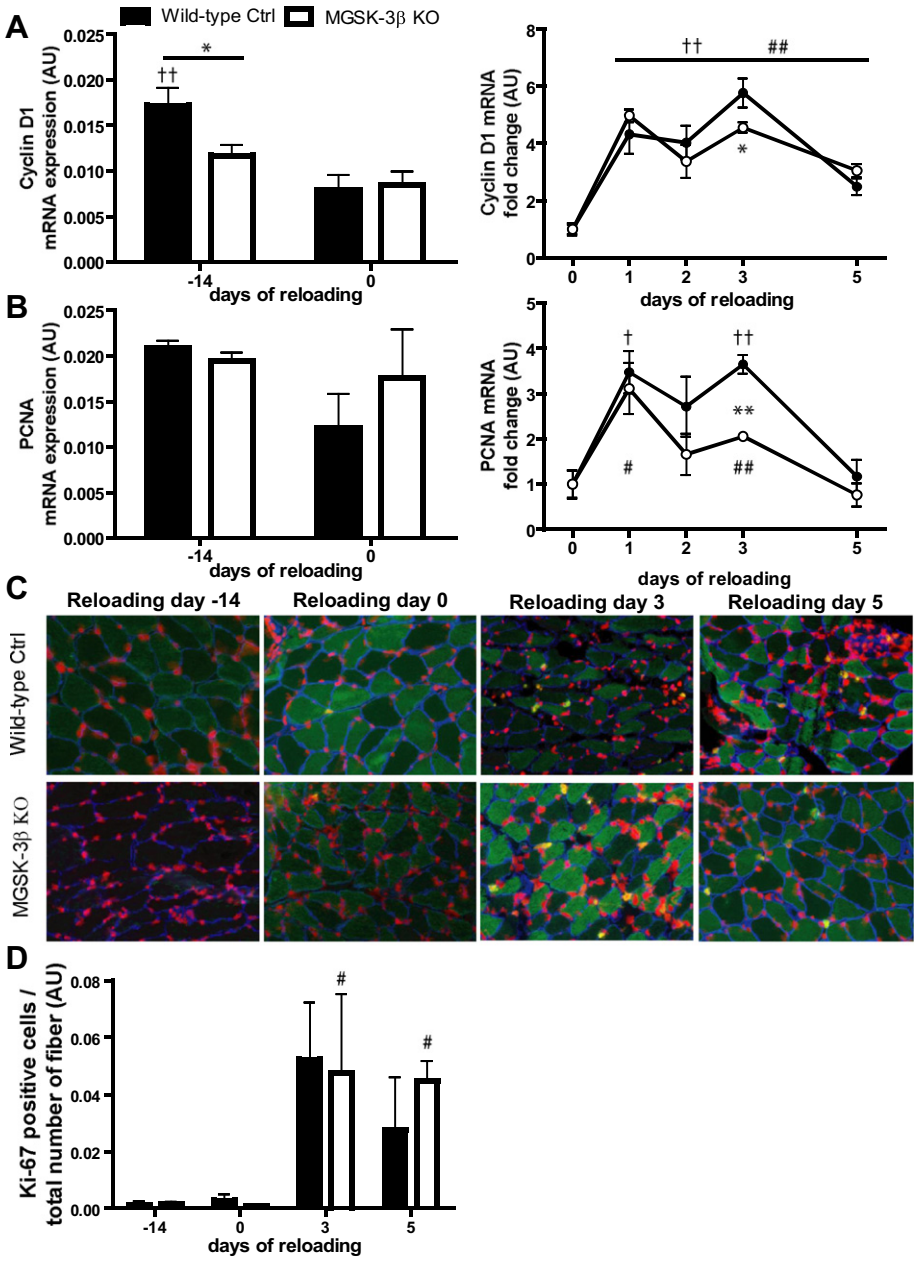

Fig. 5. Rapid induction of cell proliferation upon muscle reloading is not affected by GSK-3β ablation. M. gastrocnemius was prepared for gene expression analysis and (A) Cyclin D1 and (B) PCNA were detected to determine cell proliferation status due to HS and fold change compared to start reloading (RL-0) gene expression levels during RL (A–B group size was n = 7–9 for both WT and MGSK-3β KO). Histologically Ki-67 protein positive nuclei were determined in (C) M. soleus RL-−14 (baseline), RL-0 (HS), RL-3 and RL-5 and (D) quantified as number of positive nuclei over total number of fibers thereby identifying proliferating nuclei per section. (C group size was n = 2–4 for both WT and MGSK-3β KO). Averages ± SEM are presented, *: Wild-type Ctrl vs. MGSK-3β KO at that specific time point, †: indicates time effect compared to RL-0 (HS) for Wild-type Ctrl and #: indicates time effect compared to RL-0 (HS) for MGSK-3β KO; 1 symbol equals $p < 0.05$, 2 symbols equal $p < 0.01$, and 3 symbols equal $p < 0.001$.

and B, right panels, respectively), including the biphasic increase observed only for WT.

Muscle Regulatory Factor (MRF) Myf5 increased after HS for both WT and MGSK-3β KO (RL-0: 1.4 ± 0.1-fold, $p < 0.05$ and 1.8 ± 0.2-fold, $p < 0.01$, respectively; Fig. 6C, left panel), and did not significantly change during the subsequent RL phase. In contrast to the other two myogenic differentiation associated markers, baseline MyoD expression was lower in MGSK-3β KO compared to WT (RL-−14: 1.6-fold, $p < 0.001$; Fig. 6D, left panel). After HS MyoD expression only significantly increased in MGSK-3β KO (RL-0: 1.8 ± 0.2-fold, $p < 0.001$; Fig. 6D, left panel), abolishing the genotypic difference. MyoD expression transiently increased in WT and MGSK-3β KO on RL-1 (2.3 ± 0.5-fold, $p < 0.01$ and 2.9 ± 0.2-fold, $p < 0.001$, respectively), which was slightly more pronounced in MGSK-3β KO compared to WT muscle (1.3-fold, $p < 0.05$; Fig. 6D, right panel). Myogenin expression appeared slightly increased in WT and MGSK-3β KO muscles following HS (RL-0: 1.5 ± 0.2-fold, $p < 0.05$ and 1.6 ± 0.3-fold, $p = 0.052$, respectively; Fig. 6E, left panel). RL induced increases in myogenin expression followed a biphasic pattern in both WT and MGSK-3β KO, with marked induction on RL-1 (2.6 ± 0.3-fold, $p < 0.01$ and 5.5 ± 0.6-fold, $p < 0.001$, respectively; Fig. 6E, right panel), which was also more pronounced in MGSK-3β KO (2.1-fold, $p < 0.01$; Fig. 6E, right panel). Altogether these data revealed subtle increases in the early myogenic differentiation response during RL in regenerating muscle of MGSK-3β KO compared to WT mice.

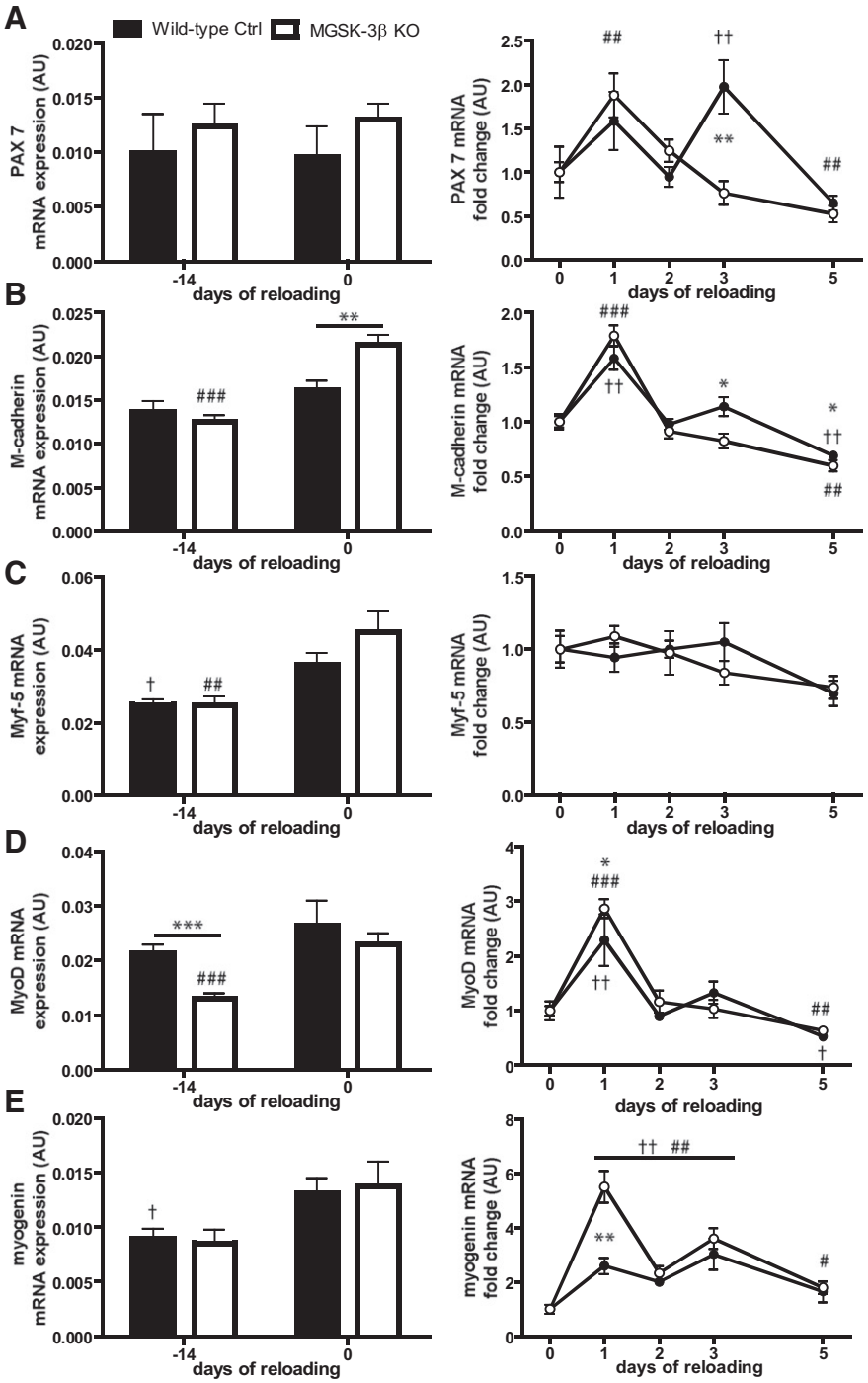

Fig. 6. Absence of GSK-3β enhances myogenesis-associated gene expression upon muscle reloading. M. gastrocnemius was prepared for gene expression analysis and (A) PAX7, (B) M-cadherin, (C) Myf5, (D) MyoD and (E) myogenin were detected to indicate satellite cell proliferation and myogenic differentiation due to HS and fold change compared to start reloading (RL-0) gene expression levels during RL. (A–E group size was n = 8 except for MGSK-3β KO RL-5 n = 7 and baseline for both genotypes n = 9). Averages ± SEM are presented, *: Wild-type Ctrl vs. MGSK-3β KO at that specific time point, †: indicates time effect compared to RL-0 (HS) for Wild-type Ctrl and #: indicates time effect compared to RL-0 (HS) for MGSK-3β KO; 1 symbol equals $p < 0.05$, 2 symbols equal $p < 0.01$, and 3 symbols equal $p < 0.001$.

3.7. GSK-3β deficiency does not prevent disuse-induced atrophy in M. soleus

Considering these consistent subtle effects of GSK-3β ablation on muscle unloading–reloading induced remodeling in M. gastrocnemius, GSK-3β-dependency of loading-induced remodeling was finally evaluated in the small, but very load-sensitive M. soleus. In line with fiber-specific recombination of the floxed GSK-3β alleles, GSK-3β protein content was ~40% decreased in M. soleus MGSK-3β KO compared to WT mice (Fig. 7A). After HS, soleus muscle weight decreased comparably in WT and MGSK-3β KO (52.1 ± 3.5%, $p < 0.001$ and 58.5 ± 3.2%, $p < 0.001$, respectively; Fig. 7B), in line with the observations in M. gastrocnemius weight loss (Fig. 1C). Correspondingly, compared to baseline, soleus muscle fiber cross sectional area (CSA) decreased

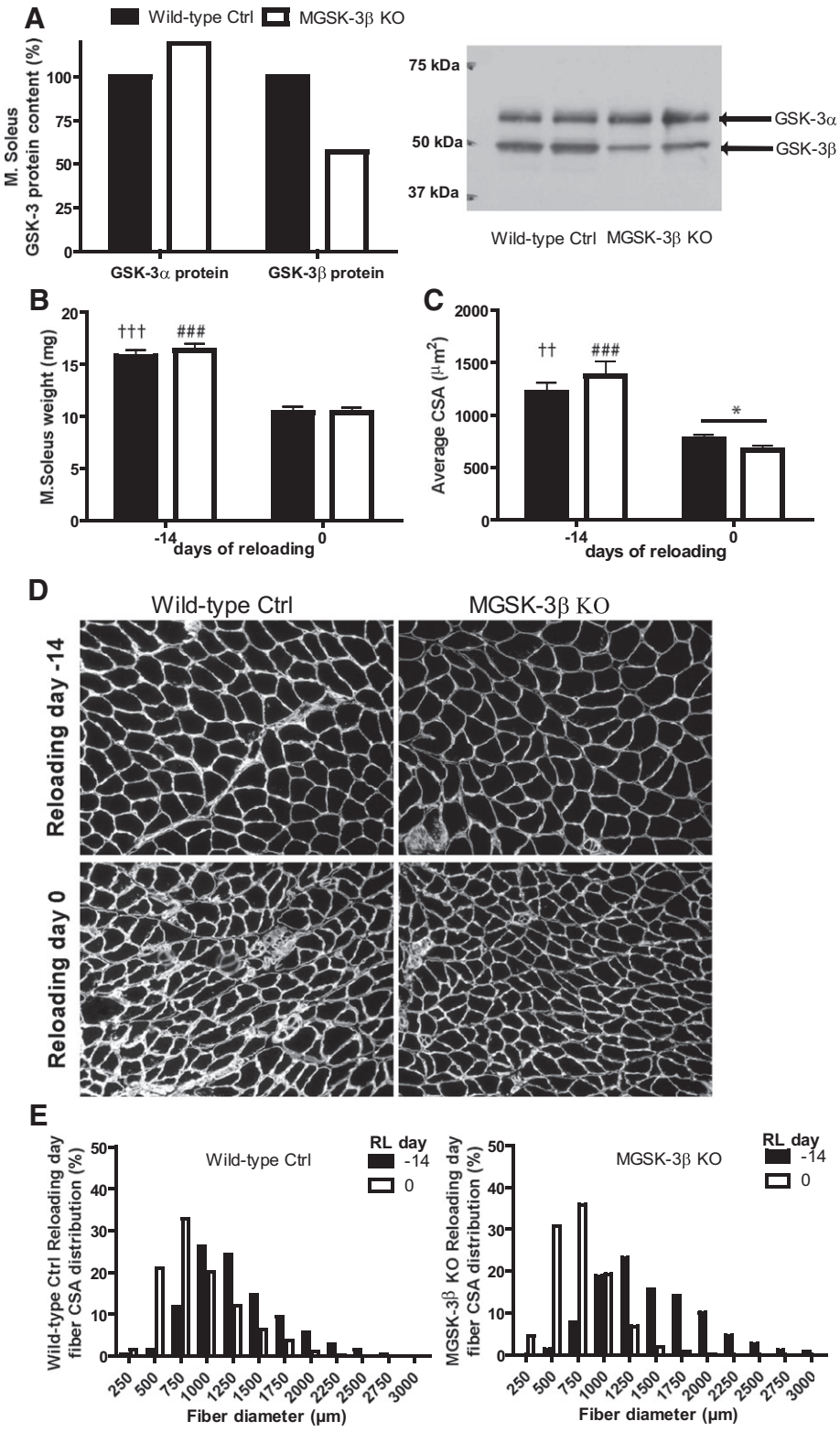

Fig. 7. GSK-3β deficiency does not prevent disuse-induced atrophy in M. soleus. (A) M. soleus protein lysates were subjected to Western blot and GSK-3β knockdown levels and GSK-3α expression levels were assessed (group size for WT/MGSK-3β KO n = 2). (B) Paired M. soleus weight loss and (C) CSA change after HS. (D) Depicted CSA changes are (E) specified for fiber size distribution change for each genotype. (B–E group size for WT and MGSK-3β KO time points RL-− 14 and RL-0 n = 8 and 5 and n = 8 and 7, respectively). Averages ± SEM are presented, *: Wild-type Ctrl vs. MGSK-3β KO at that specific time point, †: indicates time effect compared to RL-0 (HS) for Wild-type Ctrl and #: indicates time effect compared to RL-0 (HS) for MGSK-3β KO; 1 symbol equals $p < 0.05$, 2 symbols equal $p < 0.01$, and 3 symbols equal $p < 0.001$.

after HS in both WT and MGSK-3β KO mice (36.2 ± 3.3%, $p < 0.01$ and 51.6 ± 3.1%, $p < 0.001$; Fig. 7C). The CSA reduction following HS was more evident in M. soleus of MGSK-3β KO compared to WT (RL-0: − 14%, $p < 0.05$; Fig. 7C–D) following HS, which was further reflected in a slightly more leftward shift in fiber size distribution for MGSK-3β KO compared to WT (Fig. 7E).

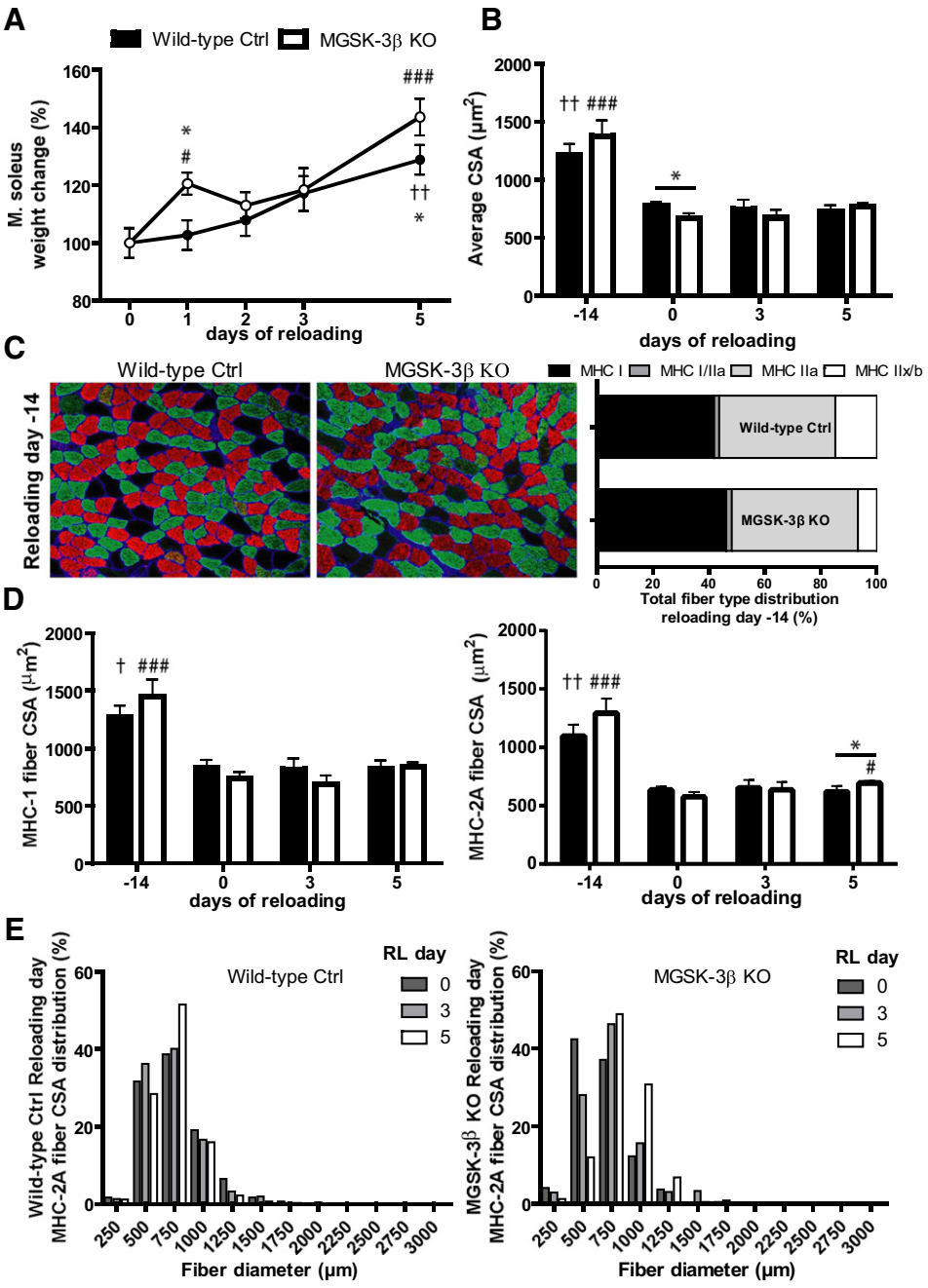

Fig. 8. Increased reloading-induced recovery of mass and fiber cross sectional area in GSK-3β deficient soleus muscle. (A) Paired M. soleus weight as a percentage increase compared to start reloading weight (RL-0) (group size was n = 8 except for MGSK-3β KO RL-5 n = 7). (B) CSA change after HS and during RL. (C) M. soleus CSA histological fiber type distribution with MHC-1 (red) and MHC-2A (green), and MHC-2X/B (black) and Laminin (blue), and represented as percentile distribution per genotype. (D) CSA change determination dependent on fiber type MHC-1 (left) and MHC-2A (right). Herein a (E) specification in MHC-2A fiber size distribution change for each genotype. (B–E group size for WT and MGSK-3β KO time points RL-−14, 0, 3 and 5 n = 8, 5, 5, 7 and n = 8, 7, 7, 6). Averages ± SEM are presented, *: Wild-type Ctrl vs. MGSK-3β KO at that specific time point, †: indicates time effect compared to RL-0 (HS) for Wild-type Ctrl and #: indicates time effect compared to RL-0 (HS) for MGSK-3β KO; 1 symbol equals $p < 0.05$, 2 symbols equal $p < 0.01$, and 3 symbols equal $p < 0.001$.

3.8. Increased reloading-induced recovery of mass and fiber cross sectional area in GSK-3β deficient soleus muscle

Soleus muscle mass increased during RL for both MGSK-3β KO and WT. However, this increase occurred more rapidly in MGSK-3β KO compared to WT mice (RL-1 vs. RL-0: 20.6 ± 3.8%, $p < 0.05$, and 2.8 ± 5.2% n.s., respectively; KO vs. WT: $p < 0.05$), and was more pronounced in MGSK-3β KO muscle (RL-5: 43.7 ± 6.4%, $p < 0.001$, and 28.9 ± 5.2%, $p < 0.01$, respectively; MGSK-3β KO vs. WT: $p < 0.05$, Fig. 8A). Remarkably, even after 5 days of RL, soleus muscle mass recovery was not accompanied by a comparable increase in muscle fiber CSA for either genotype (Fig. 8B). Nevertheless, during RL there was a trend towards increased fiber CSA compared to HS, but only in MGSK-3β KO vs. WT after 5 days of RL (15.8 ± 3.6%, $p = 0.086$ vs. −5.9 ± 6.8%, $p = 0.291$, respectively; Fig. 8B). GSK-3β levels in M. soleus were only reduced by ~40% (Fig. 7A). As this may reflect fiber type-specific recombination as a consequence of the MLC-1f promoter driven Cre-recombinase expression, CSA change during HS–RL was determined in analyses of individual fiber types according to slow or fast twitch myosin heavy chain (MHC) composition. Based on MHC-1 or -2A-immunoreactivity, these were divided into MHC-1, MHC-2A, hybrid MHC-1/MHC-2A or negative (MHC-2B and/or MHC-2X) fibers. Fiber type distribution was largely

preserved in WT and MGSK-3β KO soleus muscle, and consisted mainly out of MHC-1 and -2A fibers (Fig. 8C). MHC-1 fiber CSA did not change during RL in WT muscle, whereas a trend to increase was observed in MGSK-3β KO (RL-5: 0.1 ± 8.5%, $p = 0.808$ vs. 14.3 ± 5.9%, $p = 0.086$, respectively; Fig. 8D, left panel). Importantly, only in MGSK-3β KO muscle, MHC-2A fiber CSA significantly increased during RL (RL-5: 2.7 ± 7.6% vs. 20.6 ± 2.7%, $p < 0.05$, respectively; Fig. 8D, right panel), and MHC-2A fiber CSA at this time point was significantly ($p < 0.05$) increased in MGSK-3β KO compared to WT muscle. This difference in the recovery of MHC-2A fiber CSA during RL is further illustrated by the clear rightward shift in fiber size distribution between RL days 0–3–5 in MGSK-3β KO, but not for WT soleus muscle (Fig. 8E). These data underscore the subtle, but consistent effects of GSK-3β deficiency, indicative of accelerated muscle regeneration during recovery from disuse-induced muscle atrophy.

4. Discussion

In this study muscle specific deletion of GSK-3β (MGSK-3β KO) was used to uncover functions in muscle mass modulation that are either non-redundant with GSK-3α, or depend on total GSK-3 levels. The main hypothesis that muscle mass recovery of atrophied muscle is accelerated in the absence of GSK-3β was tested in a reversible disuse-induced muscle atrophy model. Reloading-associated changes in muscle protein turnover were not affected by the absence of GSK-3β. However, the extent and kinetics of satellite cell activation, proliferation and myogenic differentiation during reloading revealed coherent effects of GSK-3β absence, suggestive of accelerated myonuclear accretion. This was accompanied by a subtle but consistent increase in reloading-induced muscle mass accretion in GSK-3β KO muscle. Combined, these data reveal a role for GSK-3 in muscle regeneration-associated myogenesis and myonuclear accretion, independent of the regulation of muscle protein turnover, during the recovery of disuse-atrophied muscle.

Although the main hypothesis addressed in this work concerned the role of GSK-3 in muscle regeneration following unloading-induced muscle atrophy, previous work by others [102] demonstrated myotube hypertrophy in response to GSK-3 inhibition. In line, muscle-specific over-expression of IGF-I [64] correlates with GSK-3β inactivation and muscle hypertrophy [103], suggesting that the abrogation of GSK-3β may induce muscle mass and myofiber hypertrophy. Therefore, the effect of genetic ablation of muscle GSK-3β was first characterized under basal conditions.

Except for the anticipated decreased phosphorylation of eIF2Bε, no overt differences were detected in markers of protein turnover or cell proliferation and myogenic differentiation at baseline in the absence of GSK-3β. Nonetheless, MGF expression was slightly reduced in MGSK-3β KO muscle. Little information is available on the regulation of MGF transcript levels, and no previous report on effects of GSK-3 modulation on MGF expression is available. This decrease correlated with reduced Akt phosphorylation, which may suggest attenuated in vivo auto-paracrine signaling by this growth factor. Conversely, in a report by Ochi et al. increased MGF mRNA expression was accompanied by elevated Akt phosphorylation in response to exercise [104]. Although Akt signaling is inversely related to atrogene expression [105], atrogin-1 levels were lower despite reduced Akt phosphorylation in MGSK-3β KO mice. This is in line with in vitro studies revealing that in the absence of GSK-3β, the induction of protein degradation signaling resulting from Akt inhibition is markedly attenuated [75], and implicates atrogin-1 expression regulation by GSK-3β downstream of Akt.

As reduced Akt phosphorylation and atrogin-1 expression were accompanied by decreased Cyclin D1 and MyoD levels in MGSK-3β KO muscle, it is tempting to speculate that basal protein turnover and myonuclear turnover are lowered in GSK-3β ablated muscle. As atrogin-1 targets MyoD for degradation [106], lowered atrogin-1 expression may result in decreased turnover rates of MyoD protein, requiring lower MyoD mRNA expression levels to maintain MyoD protein levels. Although skeletal muscle weights did not significantly differ, there was a subtle but consistent tendency towards increased muscle mass and myofiber CSA in the reloading soleus muscle, which was more pronounced in the MHC-2A than MHC-1 fibers. Such an increase in fiber CSA in the GSK-3β KO muscle could be the consequence of increased sarcomere formation, as IGF signaling and GSK-3β inactivation stimulate this process [107]. However, it remains to be determined whether these changes translate into improved recovery of muscle function: in myostatin-depleted muscle, hypertrophy was evident but this was not accompanied by increased muscle force generation [108]. Overall, these findings are in line with a previous study in these mice in which no overt phenotypical differences on muscle and whole body mass were observed under baseline conditions [81].

Inhibition of enzymatic activity or expression of GSK-3(β) conveyed resistance to glucocorticoid-induced myotube atrophy in previous studies [75,109]. In contrast, unloading-induced gastrocnemius or soleus muscle mass loss was not prevented nor alleviated in MGSK-3β KO mice after 14 days of HS. In fact, myofiber atrophy, based on CSA analysis appeared even slightly greater in GSK-3β deficient muscle. Discrepancies between muscle weight- and fiber CSA loss have also been observed by others [110], and although these have not convincingly been addressed, differences in interstitial fluid accumulation may contribute to this phenomenon [111,112]. That GSK-3β absence did not prevent disuse-induced muscle (fiber) atrophy was contrary to our expectations. Redundancy between GSK-3α and -β may account for these results as GSK-3α levels were unaffected in MGSK-3β KO. However, Pierno et al. showed that muscle-specific IGF-I over-expression, despite resulting in muscle hypertrophy, did neither protect nor alleviated disuse-induced muscle atrophy from HS, compared to control [113], indicating that the inactivation of GSK-3, subsequent to increased IGF-I signaling, is not sufficient to prevent disuse-induced muscle atrophy. Overall, no consistent alterations in the regulation of protein or myonuclear turnover were observed in muscles of MGSK-3β KO compared to WT mice following HS; in fact only minor changes — including modestly increased atrogin-1, BNIP3 and REDD1 levels were observed in HS WT muscle compared to baseline conditions, likely reflecting a new balance in aforementioned processes associated with stabilized muscle mass following HS [114].

Nonetheless, at day two of HS, BW loss was significantly less in MGSK-3β KO compared to WT mice. During the initial phase of HS, a strong reduction in food consumption likely contributed to decrease in BW. This semi-starvation, in combination with subjection to HS itself, likely increases stress hormone release, leading to increased muscle glucocorticoid signaling [115] and subsequent muscle atrophy [116]. Interestingly, as glucocorticoid-induced muscle atrophy can be abrogated by the inhibition [109] or ablation of GSK-3β in muscles (unpublished data), the attenuated loss of BW observed in MGSK-3β KO mice, may reflect the prevention of GC-induced muscle atrophy during the initial stages of HS. However, the expression of GC-sensitive genes KLF-15 and FoXO1 [98,100] was not affected at the end of HS in WT muscle, indicating an unlikely contribution of GR signaling to disuse-induced muscle atrophy throughout HS. In line with this, denervation-induced muscle atrophy does not require GR-signaling [117]. Interestingly, this suggests overlapping GSK-3β and GR-dependency for distinct atrophy-inducing cues.

Based on previous in vitro studies by our group and others, we hypothesized that GSK-3β absence would stimulate muscle mass recovery from atrophy. In line with our hypothesis, soleus muscle mass and fiber CSA regain of MGSK-3β KO mice were enhanced compared to WT after 5 days of reloading. Conversely, the modest changes in gastrocnemius muscle weight were similar for both genotypes. This may be the consequence of the difference in sensitivity of soleus versus gastrocnemius to unloading-induced muscle atrophy leading to a greater decrease in muscle mass in soleus; therefore allowing the detection of a significant increase only in soleus muscle mass as a consequence of a more robust

response to reloading. However, regeneration-associated changes reflecting reloading-induced myonuclear accretion were detected in the gastrocnemius muscle that are more pronounced in MGSK-3β KO compared to WT.

Unexpectedly, no discernable increase in soleus fiber CSA was observed in WT and only a slight increase for MGSK-3β KO was observed after five days of reloading, despite clear increasing muscle weights for both genotypes. Similar discrepancies between muscle mass and fiber CSA changes have been observed in rats [118] and mice [110] subjected to hindlimb unloading and reloading and could be contributed to interstitial fluid accumulation during muscle regeneration [111,112]. This may in particular has contributed to very early changes in muscle mass observed after reloading, as increases in myofibrillar protein content were not detectable prior to 5 days of reloading. In line, separate analysis of MHC-1 and MHC-2A muscle fibers revealed a moderate but significant increase in MHC-2A fiber CSA within MGSK-3β KO soleus muscle only after 5 days of reloading. As Cre-mediated recombination for GSK-3β ablation is directed by the MyLC-1f promoter, which is most prominently expressed in MHC-2 type fibers, this may explain the selective increase in MHC-2A but not MHC-1 in MGSK-3β KO muscle [119]. Overall these fiber CSA data are in line with the observed accelerated muscle mass gain during RL in the absence of GSK-3β.

MGF was up-regulated in response to RL, which is in line with its postulated role in local muscle repair, maintenance and remodeling by association with the activation of satellite cell and IGF signaling [62,63]. This initial increase in MGF expression is enhanced in MGSK-3β KO muscle. IGF-I signaling influences protein synthesis [15,20–22]. Initiation of reloading (RL-1) showed a transient increase Akt phosphorylation in WT muscle, in line with literature [78,120]. However, in contrast to our previous findings in the soleus muscle [78], a significant increase in GSK-3β phosphorylation was only observed in the later phase of RL (RL-5) in the gastrocnemius muscle. The latter is consistent with the attenuated responsiveness of GSK-3β phosphorylation in the plantaris muscle [78], and could be related to the extent of atrophy a muscle is recovering from during RL. GSK-3β phosphorylation changes did not correlate with Akt phosphorylation, except for RL-5, but was inversely associated with eIF2Bε phosphorylation in WT muscle, according to literature [88]. Despite the absence of consistent changes in gastrocnemius GSK-3β or eIF2Bε phosphorylation during RL in WT muscle, both were clearly decreased in MGSK-3β KO muscle, which may have yielded a more permissive state for muscle regeneration-associated changes in protein turnover and myonuclear accretion. In addition, this also suggests a major contribution of GSK-3β relative to GSK-3α in the phosphorylation of this GSK-3 substrate, which is in line with previous estimations of the relative expression of GSK-3α and -3β [121].

In line with Akt, mTOR phosphorylation markedly increased with RL initiation, which was expected [120]. Phospho-mTOR levels remained moderately up-regulated during the course of RL, in line with the importance of mTOR related signaling for muscle recovery from disuse induced muscle atrophy previously shown by Lang et al. [122]. Similarly following literature, increased 4E-BP1 and S6K phosphorylation reflected mTOR activity and persisted throughout RL [120,122,123]. Correspondingly, REDD1 expression, a negative regulator of mTORC1 signaling [15,20,97,124,125] decreased rapidly during RL. REDD1 expression decreased more sharply in WT compared to MGSK-3β KO muscle. This likely resulted from the elevated REDD1 mRNA levels in WT at the end of HS, as mTOR-, 4E-BP1- and S6K phosphorylation were not affected by GSK-3β absence. This suggests that GSK-3β presence is not a limiting factor of translation initiation or capacity during RL-induced muscle regeneration [15,20–22]. In line with this, when GSK-3β expression was silenced in vitro using a previously described approach [75], basal or IGF-I stimulated puromycine incorporation as a measure of protein synthetic rate was not affected (data not shown). In addition, this also indicates that the regulation of S6K phosphorylation by GSK-3β, as described in vitro [126], does not apply to reloading muscle, or may point at redundant functions of GSK-3α. Of note, S6K phosphorylation revealed a clear biphasic induction, which did not correlate with changes in mTOR, but rather with Akt phosphorylation. Speculatively, this may signify the initiation of a second phase of protein synthesis, as at RL-5 muscle weights had not recovered to baseline levels. Altogether, these data do not support a non-redundant role of GSK-3β or dose-limiting effects of GSK3 in the regulation of protein synthesis signaling during reloading-induced muscle regeneration, although it cannot be ruled out that translation initiation is facilitated in MGSK3β KO muscle in case eIF2Bε activity becomes rate-limiting under conditions of markedly elevated protein synthesis.

In contrast to protein synthesis, protein degradation is expected to be decreased during RL [122,127]. FoXO is a major transcriptional regulator of muscle proteolysis [38,39,128]. Nevertheless, FoXO protein abundance only decreased after five days of reloading, which may be attributable to decreased transcription of FoXO1, as marked decreases in its mRNA transcript levels were observed; in particular in MGSK-3β KO muscle. As KLF-15 closely corresponded with FoXO1 expression levels, it is tempting to implicate KLF-15 in the transcriptional regulation of FoXO1 during HS and RL. In addition, the over-expression of KLF-15 in the tibialis muscle increases FoXO1 expression [98], but no studies previously addressed the regulation of KLF-15 or FoXO expression by GSK-3β. Increased Thr24 or Ser256 phosphorylation levels of FoXO1 corresponded with the second induction of Akt phosphorylation, suggesting the initiation of a second phase of protein synthesis with coordinated suppression of FoXO activity. Although these data do not support the regulation of FoXO phosphorylation by GSK-3β, it has been implicated in the regulation of FoXO1 transcriptional activity [129]. Genes involved in protein degradation that are transcriptionally regulated by FoXO [38,39,128] include effectors of UPS- and ALP-mediated proteolysis, i.e. atrogin-1 and MuRF1 [31,32,113], and BNIP3 [37,39,40], respectively, which are known to increase under muscle atrophying conditions [122]. As expected [122,127] both atrogin-1 and MuRF-1 mRNA expressions decreased during RL. Conversely, BNIP3 expression transiently increased, in line with literature [127], and subsequently decreased throughout further RL. Compared to the UPS markers, this differential response of BNIP3 to reloading is corresponding to the notion that autophagy is involved in the remodeling and maintenance of the skeletal muscle [130]. Although the reduction of MuRF1 and BNIP3 levels were slightly accelerated in MGSK-3β KO muscle, overall no defining role of GSK-3β absence on reloading-induced suppression of effectors of proteolysis was apparent.

These data show for the first time that muscle mass gain in response to disuse-induced muscle atrophy reloading not only involves increases in protein synthesis signaling, but that reloading is also accompanied by marked down-regulation of protein degradation signaling. Overall, these changes in protein turnover regulation were unaffected by absence of GSK-3β.

In parallel to the balance between muscle protein synthesis and degradation, myonuclear turnover may also contribute to muscle mass regulation [10]. Myonuclear accretion during muscle regeneration involves satellite cell activation, proliferation, and differentiation and fusion. Quiescent satellite cells are activated in response to muscle injury and/or exercise stimulation leading to muscle recovery [42–44]. In line with literature, PAX7 expression increased in response to exercise/muscle loading [50–52]. Activated satellite cells, once committed to myogenic differentiation become myoblasts, which fuse with existing myofibers [55] through cell–cell interaction involving M-cadherin [56–58]. Indeed, RL was accompanied by increased expression of M-cadherin. Remarkably, the biphasic induction of PAX7 and M-cadherin required GSK-3β, as only a single but more pronounced increase in their expression was observed in MGSK-3β KO muscle.

Consistent with literature, RL rapidly induced cell proliferation markers Cyclin D1, PCNA and Ki-67 in reloading muscle [110,131–133], including a second increase on RL-3, which may signify a secondary round of myogenic cell proliferation during muscle regeneration. This

matches previous reports on myogenic differentiation changes with a biphasic or greater pattern [134,135]. Although stimulating effects of GSK-3 inhibition on myogenic differentiation and myotube formation have been documented [79,136], it remained to be established whether GSK-3β ablation affects myoblast proliferation. GSK-3β suppresses Cyclin D1 expression as reviewed by Takahashi-Yanaga and Sasaguri in cancerous cells [137], whereas it is required for PCNA content in vascular smooth muscle cells [138]. This disparity in regulation may reflect a GSK-3β dependency that is determined by cellular context. In the reloading muscle, expression patterns of Cyclin D1 and PCNA changed coordinately, and were impacted similarly by the absence of GSK-3β: GSK-3β ablation blunted the secondary expression increase of both proliferation markers. Importantly, the identical GSK-3β-dependency on biphasic increases in satellite cell activation and proliferation markers during RL supports the notion that the latter reflects dividing myoblasts and no other resident cell-types. Moreover, since GSK-3β suppression did not directly affect the expression of proliferation markers but rather promoted myogenic differentiation of cultured myoblasts [136], the relative suppression of PCNA and Cyclin D1 expression at day 3 may point at accelerated myogenesis in the absence of GSK-3β.

Subsequent myogenic differentiation of myoblasts includes increased muscle-specific gene expression, regulated by the MRFs Myf-5, MyoD and myogenin [59,60]. Myf-5 expression, suggested to be involved in satellite cell proliferation [139], was unaffected by RL or GSK-3β absence. MyoD and myogenin increase during RL, which is in line with literature [120,132]. Interestingly, early up-regulation of MyoD and especially myogenin was markedly increased in MGSK-3β KO compared to WT regenerating muscle, which is consistent with the stimulation of myogenic differentiation in response to GSK-3 inhibition observed in a previous in vitro report [65].

Of interest, satellite cell activation and myoblast proliferation revealed a biphasic response, which preceded the secondary rise in protein synthesis signaling, i.e. increased phosphorylation of Akt, and S6K on RL-5, suggesting coordinated control of muscle protein synthesis and proliferation signaling. This possible second rise of satellite cell activation and proliferation markers was absent in MGSK-3β KO muscle, whereas the initial rise in MGF expression and myogenic differentiation markers was clearly more pronounced in MGSK-3β KO muscle. This may suggest that a second round of satellite cell activation and proliferation may not be required in MGSK-3β KO muscle as a consequence of more extensive myogenic differentiation of the initially activated and recruited satellite cells. In agreement with this notion, muscle mass and myofiber CSA increases were not blunted, but even slightly enhanced in MGSK-3β KO muscle. However, this could have potential implications for the replenishment of the quiescent satellite cell pool, considering the requirement for asymmetrical cell division postulated to confer sustained myogenic potential of the skeletal muscle in muscle mass maintenance [140]. In congruence with this idea, the absence of GSK-3α was recently postulated to accelerate aging of multiple tissues including the skeletal muscle [141].

All the potentiating effects of GSK-3β deletion on the initial stages of molecular myogenic differentiation, reloading-induced muscle mass and myofiber CSA recovery were subtle. However, this does not rule out further attention for GSK-3 as a nexus in skeletal muscle mass plasticity. We previously reported that reloading of disuse-induced atrophied soleus muscle mass recovery is accompanied by increased inactivating GSK-3β phosphorylation [78]. Under physiological healthy conditions reloading may suppress GSK-3 activity levels sufficiently to accommodate muscle recovery. However, whether such reduction in GSK-3 activity is required for efficient recovery remains to be addressed; especially as aberrant GSK-3 regulation has been associated with impaired muscle mass plasticity [142–144]. Moreover, putative beneficial effects of modulating GSK-3 activity may vary between different triggers of muscle atrophy, and subsequent recovery conditions. To illustrate this, the systemic delivery of a GSK-3β inhibitor was recently found to attenuate muscle atrophy in a model of chronic pulmonary inflammation, and improve cytokine- or glucocorticoid-induced inhibition of myogenic differentiation [145].

In conclusion, GSK-3β deletion potentiates the initiation of the molecular response underlying myonuclear accretion, resulting in enhanced muscle mass and fiber CSA gain. This study therefore suggests that GSK-3β specific, non-redundant functions with GSK-3α, or total GSK-3 (activity) levels suppress muscle regeneration during the recovery of disuse-atrophy.

Conflict of interests

No conflicts of interest, financial or otherwise, are declared by the author(s).

Acknowledgements

We would like to thank both Satish Patel and Jim R. Woodgett for providing us with the skeletal muscle-specific (M)GSK-3β KO C57/Bl6 mouse strain and reviewing and comments on this manuscript. This work was supported by a grant from the Lung Foundation/Netherlands Asthma Foundation (NAF 3.2.07.017) and the Transnational University Limburg (tUL), without any further involvement in the execution of the presented work.

References

[1] S.D. Anker, et al., Wasting as independent risk factor for mortality in chronic heart failure, Lancet 349 (9058) (1997) 1050–1053.
[2] L. Altomonte, et al., Serum levels of interleukin-1b, tumour necrosis factor-a and interleukin-2 in rheumatoid arthritis. Correlation with disease activity, Clin. Rheumatol. 11 (2) (1992) 202–205.
[3] R. Roubenoff, et al., Rheumatoid cachexia: cytokine-driven hypermetabolism accompanying reduced body cell mass in chronic inflammation, J. Clin. Invest. 93 (6) (1994) 2379–2386.
[4] H. Valdez, M.M. Lederman, Cytokines and cytokine therapies in HIV infection, AIDS Clin. Rev. (1997) 187–228.
[5] A.M. Schols, et al., Weight loss is a reversible factor in the prognosis of chronic obstructive pulmonary disease, Am. J. Respir. Crit. Care Med. 157 (6 Pt 1) (1998) 1791–1797.
[6] R. Debigare, C.H. Cote, F. Maltais, Peripheral muscle wasting in chronic obstructive pulmonary disease. Clinical relevance and mechanisms, Am. J. Respir. Crit. Care Med. 164 (9) (2001) 1712–1717.
[7] J.M. Argiles, F.J. Lopez-Soriano, The role of cytokines in cancer cachexia, Med. Res. Rev. 19 (3) (1999) 223–248.
[8] K. Fearon, et al., Definition and classification of cancer cachexia: an international consensus, Lancet Oncol. 12 (5) (2011) 489–495.
[9] A.M. Schols, et al., Body composition and mortality in chronic obstructive pulmonary disease, Am. J. Clin. Nutr. 82 (1) (2005) 53–59.
[10] C.A. Goodman, D.L. Mayhew, T.A. Hornberger, Recent progress toward understanding the molecular mechanisms that regulate skeletal muscle mass, Cell. Signal. 23 (12) (2011) 1896–1906.
[11] D.D. Sarbassov, et al., Phosphorylation and regulation of Akt/PKB by the rictor-mTOR complex, Science 307 (5712) (2005) 1098–1101.
[12] D.R. Alessi, et al., Mechanism of activation of protein kinase B by insulin and IGF-1, EMBO J. 15 (23) (1996) 6541–6551.
[13] E. Jacinto, et al., SIN1/MIP1 maintains rictor–mTOR complex integrity and regulates Akt phosphorylation and substrate specificity, Cell 127 (1) (2006) 125–137.
[14] T.N. Stitt, et al., The IGF-1/PI3K/Akt pathway prevents expression of muscle atrophy-induced ubiquitin ligases by inhibiting FOXO transcription factors, Mol. Cell 14 (3) (2004) 395–403.
[15] R.A. Frost, et al., Regulation of REDD1 by insulin-like growth factor-I in skeletal muscle and myotubes, J. Cell. Biochem. 108 (5) (2009) 1192–1202.
[16] D.A. Cross, et al., Inhibition of glycogen synthase kinase-3 by insulin mediated by protein kinase B, Nature 378 (6559) (1995) 785–789.
[17] K.J. Verhees, et al., Regulation of skeletal muscle plasticity by glycogen synthase kinase-3beta: a potential target for the treatment of muscle wasting, Curr. Pharm. Des. 19 (18) (2013) 3276–3298.
[18] S.C. Bodine, et al., Akt/mTOR pathway is a crucial regulator of skeletal muscle hypertrophy and can prevent muscle atrophy in vivo, Nat. Cell Biol. 3 (11) (2001) 1014–1019.
[19] S.C. Kandarian, R.W. Jackman, Intracellular signaling during skeletal muscle atrophy, Muscle Nerve 33 (2) (2006) 155–165.
[20] H. Wang, et al., Dexamethasone represses signaling through the mammalian target of rapamycin in muscle cells by enhancing expression of REDD1, J. Biol. Chem. 281 (51) (2006) 39128–39134.
[21] W. Qin, et al., Protection against dexamethasone-induced muscle atrophy is related to modulation by testosterone of FOXO1 and PGC-1alpha, Biochem. Biophys. Res. Commun. 403 (3–4) (2010) 473–478.

[22] B.G. Li, P.O. Hasselgren, C.H. Fang, Insulin-like growth factor-I inhibits dexamethasone-induced proteolysis in cultured L6 myotubes through PI3K/Akt/GSK-3beta and PI3K/Akt/mTOR-dependent mechanisms, Int. J. Biochem. Cell Biol. 37 (10) (2005) 2207–2216.
[23] L.S. Jefferson, J.R. Fabian, S.R. Kimball, Glycogen synthase kinase-3 is the predominant insulin-regulated eukaryotic initiation factor 2B kinase in skeletal muscle, Int. J. Biochem. Cell Biol. 31 (1) (1999) 191–200.
[24] G.I. Welsh, C.G. Proud, Glycogen synthase kinase-3 is rapidly inactivated in response to insulin and phosphorylates eukaryotic initiation factor eIF-2B, Biochem. J. 294 (Pt 3) (1993) 625–629.
[25] S.R. Kimball, L.S. Jefferson, Control of translation initiation through integration of signals generated by hormones, nutrients, and exercise, J. Biol. Chem. 285 (38) (2010) 29027–29032.
[26] S.E. Hardt, J. Sadoshima, Glycogen synthase kinase-3 beta: a novel regulator of cardiac hypertrophy and development, Circ. Res. 90 (10) (2002) 1055–1063.
[27] E.E. Dupont-Versteegden, Apoptosis in skeletal muscle and its relevance to atrophy, World J. Gastroenterol. 12 (46) (2006) 7463–7466.
[28] I.J. Smith, S.H. Lecker, P.O. Hasselgren, Calpain activity and muscle wasting in sepsis, Am. J. Physiol. Endocrinol. Metab. 295 (4) (2008) E762–E771.
[29] A. Ciechanover, A. Orian, A.L. Schwartz, Ubiquitin-mediated proteolysis: biological regulation via destruction, Bioessays 22 (5) (2000) 442–451.
[30] A.L. Schwartz, A. Ciechanover, Targeting proteins for destruction by the ubiquitin system: implications for human pathobiology, Annu. Rev. Pharmacol. Toxicol. 49 (2009) 73–96.
[31] J.M. Sacheck, et al., Rapid disuse and denervation atrophy involve transcriptional changes similar to those of muscle wasting during systemic diseases, FASEB J. 21 (1) (2007) 140–155.
[32] C.J. Wray, et al., Sepsis upregulates the gene expression of multiple ubiquitin ligases in skeletal muscle, Int. J. Biochem. Cell Biol. 35 (5) (2003) 698–705.
[33] B.A. Clarke, et al., The E3 Ligase MuRF1 degrades myosin heavy chain protein in dexamethasone-treated skeletal muscle, Cell Metab. 6 (5) (2007) 376–385.
[34] T.J. Zhao, et al., The generation of the oxidized form of creatine kinase is a negative regulation on muscle creatine kinase, J. Biol. Chem. 282 (16) (2007) 12022–12029.
[35] S. Cohen, et al., During muscle atrophy, thick, but not thin, filament components are degraded by MuRF1-dependent ubiquitylation, J. Cell Biol. 185 (6) (2009) 1083–1095.
[36] J. Lagirand-Cantaloube, et al., Inhibition of atrogin-1/MAFbx mediated MyoD proteolysis prevents skeletal muscle atrophy in vivo, PLoS One 4 (3) (2009) e4973.
[37] M. Sandri, Autophagy in health and disease. 3. Involvement of autophagy in muscle atrophy, Am. J. Physiol. Cell Physiol. 298 (6) (2010) C1291–C1297.
[38] T.J. McLoughlin, et al., FoxO1 induces apoptosis in skeletal myotubes in a DNA binding-dependent manner, Am. J. Physiol. Cell Physiol. 297 (3) (2009) C548–C555.
[39] M. Sandri, et al., Foxo transcription factors induce the atrophy-related ubiquitin ligase atrogin-1 and cause skeletal muscle atrophy, Cell 117 (3) (2004) 399–412.
[40] J. Zhao, et al., FoxO3 coordinately activates protein degradation by the autophagic/lysosomal and proteasomal pathways in atrophying muscle cells, Cell Metab. 6 (6) (2007) 472–483.
[41] A. Mauro, Satellite cell of skeletal muscle fibers, J. Biophys. Biochem. Cytol. 9 (1961) 493–495.
[42] J.E. Morgan, T.A. Partridge, Muscle satellite cells, Int. J. Biochem. Cell Biol. 35 (8) (2003) 1151–1156.
[43] J.D. Rosenblatt, D. Yong, D.J. Parry, Satellite cell activity is required for hypertrophy of overloaded adult rat muscle, Muscle Nerve 17 (6) (1994) 608–613.
[44] F. Relaix, P.S. Zammit, Satellite cells are essential for skeletal muscle regeneration: the cell on the edge returns centre stage, Development 139 (16) (2012) 2845–2856.
[45] G. Vescovo, et al., Apoptosis in the skeletal muscle of patients with heart failure: investigation of clinical and biochemical changes, Heart 84 (4) (2000) 431–437.
[46] M.I. Lewis, Apoptosis as a potential mechanism of muscle cachexia in chronic obstructive pulmonary disease, Am. J. Respir. Crit. Care Med. 166 (4) (2002) 434–436.
[47] X. Zhou, et al., Reversal of cancer cachexia and muscle wasting by ActRIIB antagonism leads to prolonged survival, Cell 142 (4) (2010) 531–543.
[48] D.L. Allen, et al., Apoptosis: a mechanism contributing to remodeling of skeletal muscle in response to hindlimb unweighting, Am. J. Physiol. 273 (2 Pt 1) (1997) C579–C587.
[49] A.J. Dirks-Naylor, S. Lennon-Edwards, Cellular and molecular mechanisms of apoptosis in age-related muscle atrophy, Curr. Aging Sci. 4 (3) (2011) 269–278.
[50] F. Relaix, et al., Pax3 and Pax7 have distinct and overlapping functions in adult muscle progenitor cells, J. Cell Biol. 172 (1) (2006) 91–102.
[51] F. Relaix, et al., A Pax3/Pax7-dependent population of skeletal muscle progenitor cells, Nature 435 (7044) (2005) 948–953.
[52] R. Sambasivan, et al., Pax7-expressing satellite cells are indispensable for adult skeletal muscle regeneration, Development 138 (17) (2011) 3647–3656.
[53] A.L. Mackey, et al., Assessment of satellite cell number and activity status in human skeletal muscle biopsies, Muscle Nerve 40 (3) (2009) 455–465.
[54] E. Castillero, et al., IGF-I system, atrogenes and myogenic regulatory factors in arthritis induced muscle wasting, Mol. Cell. Endocrinol. 309 (1–2) (2009) 8–16.
[55] T.J. Hawke, D.J. Garry, Myogenic satellite cells: physiology to molecular biology, J. Appl. Physiol. (1985) 91 (2) (2001) 534–551.
[56] E. Wrobel, E. Brzoska, J. Moraczewski, M-cadherin and beta-catenin participate in differentiation of rat satellite cells, Eur. J. Cell Biol. 86 (2) (2007) 99–109.
[57] I. Kramerova, et al., Regulation of the M-cadherin–beta-catenin complex by calpain 3 during terminal stages of myogenic differentiation, Mol. Cell. Biol. 26 (22) (2006) 8437–8447.
[58] M. Ishido, et al., Alterations of M-cadherin, neural cell adhesion molecule and beta-catenin expression in satellite cells during overload-induced skeletal muscle hypertrophy, Acta. Physiol. (Oxf.) 187 (3) (2006) 407–418.
[59] M.A. Rudnicki, R. Jaenisch, The MyoD family of transcription factors and skeletal myogenesis, Bioessays 17 (3) (1995) 203–209.
[60] J.S. Kang, R.S. Krauss, Muscle stem cells in developmental and regenerative myogenesis, Curr. Opin. Clin. Nutr. Metab. Care 13 (3) (2010) 243–248.
[61] R.W. Matheny Jr., B.C. Nindl, M.L. Adamo, Minireview: mechano-growth factor: a putative product of IGF-I gene expression involved in tissue repair and regeneration, Endocrinology 151 (3) (2010) 865–875.
[62] M. Hill, G. Goldspink, Expression and splicing of the insulin-like growth factor gene in rodent muscle is associated with muscle satellite (stem) cell activation following local tissue damage, J. Physiol. 549 (Pt 2) (2003) 409–418.
[63] V. Owino, S.Y. Yang, G. Goldspink, Age-related loss of skeletal muscle function and the inability to express the autocrine form of insulin-like growth factor-1 (MGF) in response to mechanical overload, FEBS Lett. 505 (2) (2001) 259–263.
[64] A. Musaro, et al., Localized Igf-1 transgene expression sustains hypertrophy and regeneration in senescent skeletal muscle, Nat. Genet. 27 (2) (2001) 195–200.
[65] J.L. van der Velden, et al., Inhibition of glycogen synthase kinase-3beta activity is sufficient to stimulate myogenic differentiation, Am. J. Physiol. Cell Physiol. 290 (2) (2006) C453–C462.
[66] N.A. Pansters, et al., Synergistic stimulation of myogenesis by glucocorticoid and IGF-I signaling, J. Appl. Physiol. (1985) 114 (9) (2013) 1329–1339.
[67] T. Yoshida, et al., IGF-1 prevents ANG II-induced skeletal muscle atrophy via Akt- and Foxo-dependent inhibition of the ubiquitin ligase atrogin-1 expression, Am. J. Physiol. Heart Circ. Physiol. 298 (2010) H1565–H1570.
[68] L. Pelosi, et al., Local expression of IGF-1 accelerates muscle regeneration by rapidly modulating inflammatory cytokines and chemokines, FASEB J. 21 (7) (2007) 1393–1402.
[69] J.R. Florini, D.Z. Ewton, S.A. Coolican, Growth hormone and the insulin-like growth factor system in myogenesis, Endocr. Rev. 17 (5) (1996) 481–517.
[70] C. Duan, H. Ren, S. Gao, Insulin-like growth factors (IGFs), IGF receptors, and IGF-binding proteins: roles in skeletal muscle growth and differentiation, Gen. Comp. Endocrinol. 167 (3) (2010) 344–351.
[71] D.R. Clemmons, Role of IGF-I in skeletal muscle mass maintenance, Trends Endocrinol. Metab. 20 (7) (2009) 349–356.
[72] R.A. Frost, C.H. Lang, Protein kinase B/Akt: a nexus of growth factor and cytokine signaling in determining muscle mass, J. Appl. Physiol. 103 (1) (2007) 378–387.
[73] G.A. Nader, Molecular determinants of skeletal muscle mass: getting the "AKT" together, Int. J. Biochem. Cell Biol. 37 (10) (2005) 1985–1996.
[74] M. Wu, M. Falasca, E.R. Blough, Akt/protein kinase B in skeletal muscle physiology and pathology, J. Cell. Physiol. 226 (1) (2010) 29–36.
[75] K.J. Verhees, et al., Glycogen synthase kinase-3beta is required for the induction of skeletal muscle atrophy, Am. J. Physiol. Cell Physiol. 301 (5) (2011) C995–C1007.
[76] A.R. Evenson, et al., GSK-3beta inhibitors reduce protein degradation in muscles from septic rats and in dexamethasone-treated myotubes, Int. J. Biochem. Cell Biol. 37 (10) (2005) 2226–2238.
[77] C.H. Fang, et al., GSK-3beta activity is increased in skeletal muscle after burn injury in rats, Am. J. Physiol. Regul. Integr. Comp. Physiol. 293 (4) (2007) R1545–R1551.
[78] J.L. van der Velden, et al., Myogenic differentiation during regrowth of atrophied skeletal muscle is associated with inactivation of GSK-3beta, Am. J. Physiol. Cell Physiol. 292 (5) (2007) C1636–C1644.
[79] J.L. van der Velden, et al., Glycogen synthase kinase 3 suppresses myogenic differentiation through negative regulation of NFATc3, J. Biol. Chem. 283 (1) (2008) 358–366.
[80] R.C. Langen, et al., Triggers and mechanisms of skeletal muscle wasting in chronic obstructive pulmonary disease, Int. J. Biochem. Cell Biol. 45 (10) (2013) 2245–2256.
[81] S. Patel, et al., Tissue-specific role of glycogen synthase kinase 3beta in glucose homeostasis and insulin action, Mol. Cell. Biol. 28 (20) (2008) 6314–6328.
[82] P.O. Mitchell, G.K. Pavlath, A muscle precursor cell-dependent pathway contributes to muscle growth after atrophy, Am. J. Physiol. Cell Physiol. 281 (5) (2001) C1706–C1715.
[83] R.C. Langen, et al., Tumor necrosis factor-alpha inhibits myogenic differentiation through MyoD protein destabilization, FASEB J. 18 (2) (2004) 227–237.
[84] J. Vandesompele, et al., Accurate normalization of real-time quantitative RT-PCR data by geometric averaging of multiple internal control genes, Genome Biol. 3 (7) (2002) (p. RESEARCH0034).
[85] K.M. Heinemeier, et al., Effect of unloading followed by reloading on expression of collagen and related growth factors in rat tendon and muscle, J. Appl. Physiol. (1985) 106 (1) (2009) 178–186.
[86] D. Bloemberg, J. Quadrilatero, Rapid determination of myosin heavy chain expression in rat, mouse, and human skeletal muscle using multicolor immunofluorescence analysis, PLoS One 7 (4) (2012) e35273.
[87] J.M. Steffen, et al., A suspension model for hypokinetic/hypodynamic and antiorthostatic responses in the mouse, Aviat. Space Environ. Med. 55 (7) (1984) 612–616.
[88] G.I. Welsh, et al., Regulation of eukaryotic initiation factor eIF2B: glycogen synthase kinase-3 phosphorylates a conserved serine which undergoes dephosphorylation in response to insulin, FEBS Lett. 421 (2) (1998) 125–130.
[89] G. Goldspink, Changes in muscle mass and phenotype and the expression of autocrine and systemic growth factors by muscle in response to stretch and overload, J. Anat. 194 (Pt 3) (1999) 323–334.
[90] A.M. Hanson, et al., Longitudinal characterization of functional, morphologic, and biochemical adaptations in mouse skeletal muscle with hindlimb suspension, Muscle Nerve 48 (3) (2013) 393–402.
[91] C.A. Goodman, et al., The role of skeletal muscle mTOR in the regulation of mechanical load-induced growth, J. Physiol. 589 (Pt 22) (2011) 5485–5501.
[92] M. Fluck, et al., Transcriptional reprogramming during reloading of atrophied rat soleus muscle, Am. J. Physiol. Regul. Integr. Comp. Physiol. 289 (1) (2005) R4–R14.

[93] D.S. Waddell, et al., The glucocorticoid receptor and FOXO1 synergistically activate the skeletal muscle atrophy-associated MuRF1 gene, Am. J. Physiol. Endocrinol. Metab. 295 (4) (2008) E785–E797.
[94] O. Schakman, H. Gilson, J.P. Thissen, Mechanisms of glucocorticoid-induced myopathy, J. Endocrinol. 197 (1) (2008) 1–10.
[95] Z. Hu, et al., Endogenous glucocorticoids and impaired insulin signaling are both required to stimulate muscle wasting under pathophysiological conditions in mice, J. Clin. Invest. 119 (10) (2009) 3059–3069.
[96] M. Menconi, et al., Role of glucocorticoids in the molecular regulation of muscle wasting, Crit. Care Med. 35 (9 Suppl.) (2007) S602–S608.
[97] R. Kumari, et al., REDD1 (regulated in development and DNA damage response 1) expression in skeletal muscle as a surrogate biomarker of the efficiency of glucocorticoid receptor blockade, Biochem. Biophys. Res. Commun. 412 (4) (2011) 644–647.
[98] N. Shimizu, et al., Crosstalk between glucocorticoid receptor and nutritional sensor mTOR in skeletal muscle, Cell Metab. 13 (2) (2011) 170–182.
[99] N. Yoshikawa, et al., Ligand-based gene expression profiling reveals novel roles of glucocorticoid receptor in cardiac metabolism, Am. J. Physiol. Endocrinol. Metab. 296 (6) (2009) E1363–E1373.
[100] J.E. Cho, et al., 2009, Time course expression of Foxo transcription factors in skeletal muscle following corticosteroid administration, J. Appl. Physiol 108 (1) (1985) 137–145.
[101] L.P. van der Heide, M.F. Hoekman, M.P. Smidt, The ins and outs of FoxO shuttling: mechanisms of FoxO translocation and transcriptional regulation, Biochem. J. 380 (Pt 2) (2004) 297–309.
[102] D.R. Vyas, et al., GSK-3beta negatively regulates skeletal myotube hypertrophy, Am. J. Physiol. Cell Physiol. 283 (2) (2002) C545–C551.
[103] C. Rommel, et al., Mediation of IGF-1-induced skeletal myotube hypertrophy by PI(3)K/Akt/mTOR and PI(3)K/Akt/GSK3 pathways, Nat. Cell Biol. 3 (11) (2001) 1009–1013.
[104] E. Ochi, N. Ishii, K. Nakazato, Time course change of IGF1/Akt/mTOR/p70s6k pathway activation in rat gastrocnemius muscle during repeated bouts of eccentric exercise, J. Sports Sci. Med. 9 (2) (2010) 170–175.
[105] E. Latres, et al., Insulin-like growth factor-1 (IGF-1) inversely regulates atrophy-induced genes via the phosphatidylinositol 3-kinase/Akt/mammalian target of rapamycin (PI3K/Akt/mTOR) pathway, J. Biol. Chem. 280 (4) (2005) 2737–2744.
[106] L.A. Tintignac, et al., Degradation of MyoD mediated by the SCF (MAFbx) ubiquitin ligase, J. Biol. Chem. 280 (4) (2005) 2847–2856.
[107] K. Takano, et al., Nebulin and N-WASP cooperate to cause IGF-1-induced sarcomeric actin filament formation, Science 330 (6010) (2010) 1536–1540.
[108] K.E. Personius, et al., Grip force, EDL contractile properties, and voluntary wheel running after postdevelopmental myostatin depletion in mice, J. Appl. Physiol. (1985) 109 (3) (2010) 886–894.
[109] O. Schakman, et al., Role of Akt/GSK-3beta/beta-catenin transduction pathway in the muscle anti-atrophy action of insulin-like growth factor-I in glucocorticoid-treated rats, Endocrinology 149 (8) (2008) 3900–3908.
[110] J.R. Jackson, et al., Satellite cell depletion does not inhibit adult skeletal muscle regrowth following unloading-induced atrophy, Am. J. Physiol. Cell Physiol. 303 (8) (2012) C854–C861.
[111] M.J. Warhol, et al., Skeletal muscle injury and repair in marathon runners after competition, Am. J. Pathol. 118 (2) (1985) 331–339.
[112] T.L. Criswell, et al., Compression-induced muscle injury in rats that mimics compartment syndrome in humans, Am. J. Pathol. 180 (2) (2012) 787–797.
[113] S. Pierno, et al., Paracrine effects of IGF-1 overexpression on the functional decline due to skeletal muscle disuse: molecular and functional evaluation in hindlimb unloaded MLC/mIgf-1 transgenic mice, PLoS One 8 (6) (2013) e65167.
[114] R.C. Langen, et al., Muscle wasting and impaired muscle regeneration in a murine model of chronic pulmonary inflammation, Am. J. Respir. Cell Mol. Biol. 35 (6) (2006) 689–696.
[115] T. Kuo, C.A. Harris, J.C. Wang, Metabolic functions of glucocorticoid receptor in skeletal muscle, Mol. Cell. Endocrinol. 380 (1–2) (2013) 79–88.
[116] M.A. Pellegrino, et al., Clenbuterol antagonizes glucocorticoid-induced atrophy and fibre type transformation in mice, Exp. Physiol. 89 (1) (2004) 89–100.
[117] M.L. Watson, et al., A cell-autonomous role for the glucocorticoid receptor in skeletal muscle atrophy induced by systemic glucocorticoid exposure, Am. J. Physiol. Endocrinol. Metab. 302 (10) (2012) E1210–E1220.
[118] J.J. Widrick, et al., Detrimental effects of reloading recovery on force, shortening velocity, and power of soleus muscles from hindlimb-unloaded rats, Am. J. Physiol. Regul. Integr. Comp. Physiol. 295 (5) (2008) R1585–R1592.
[119] M.J. Donoghue, et al., Fiber type- and position-dependent expression of a myosin light chain-CAT transgene detected with a novel histochemical stain for CAT, J. Cell Biol. 115 (2) (1991) 423–434.
[120] T.A. Washington, et al., Skeletal muscle mass recovery from atrophy in IL-6 knockout mice, Acta Physiol. (Oxf.) 202 (4) (2011) 657–669.
[121] E.J. McManus, et al., Role that phosphorylation of GSK3 plays in insulin and Wnt signalling defined by knockin analysis, EMBO J. 24 (8) (2005) 1571–1583.
[122] S.M. Lang, et al., Delayed recovery of skeletal muscle mass following hindlimb immobilization in mTOR heterozygous mice, PLoS One 7 (6) (2012) e38910.
[123] T.E. Childs, et al., Temporal alterations in protein signaling cascades during recovery from muscle atrophy, Am. J. Physiol. Cell Physiol. 285 (2) (2003) C391–C398.
[124] O.J. Shah, S.R. Kimball, L.S. Jefferson, Acute attenuation of translation initiation and protein synthesis by glucocorticoids in skeletal muscle, Am. J. Physiol. Endocrinol. Metab. 278 (1) (2000) E76–E82.
[125] K. Masuno, et al., Expression profiling identifies Klf15 as a glucocorticoid target that regulates airway hyperresponsiveness, Am. J. Respir. Cell Mol. Biol. 45 (3) (2011) 642–649.
[126] S. Shin, et al., Glycogen synthase kinase (GSK)-3 promotes p70 ribosomal protein S6 kinase (p70S6K) activity and cell proliferation, Proc. Natl. Acad. Sci. U. S. A. 108 (47) (2011) E1204–E1213.
[127] T. Andrianjafiniony, et al., Oxidative stress, apoptosis, and proteolysis in skeletal muscle repair after unloading, Am. J. Physiol. Cell Physiol. 299 (2) (2010) C307–C315.
[128] B. Zheng, et al., FOXO3a mediates signaling crosstalk that coordinates ubiquitin and atrogin-1/MAFbx expression during glucocorticoid-induced skeletal muscle atrophy, FASEB J. 24 (8) (2010) 2660–2669.
[129] J. Sakamaki, et al., GSK3beta regulates gluconeogenic gene expression through HNF4alpha and FOXO1, J. Recept. Signal Transduct. Res. 32 (2) (2012) 96–101.
[130] E. Masiero, et al., Autophagy is required to maintain muscle mass, Cell Metab. 10 (6) (2009) 507–515.
[131] M.D. Roberts, et al., Effects of preexercise feeding on markers of satellite cell activation, Med. Sci. Sports Exerc. 42 (10) (2010) 1861–1869.
[132] S.E. Alway, et al., beta-Hydroxy-beta-methylbutyrate (HMB) enhances the proliferation of satellite cells in fast muscles of aged rats during recovery from disuse atrophy, Exp. Gerontol. 48 (9) (2013) 973–984.
[133] B. Crassous, et al., Lack of effects of creatine on the regeneration of soleus muscle after injury in rats, Med. Sci. Sports Exerc. 41 (9) (2009) 1761–1769.
[134] K. Takeuchi, et al., Heat stress promotes skeletal muscle regeneration after crush injury in rats, Acta Histochem. 116 (2) (2014) 327–334.
[135] Z. Yan, et al., Highly coordinated gene regulation in mouse skeletal muscle regeneration, J. Biol. Chem. 278 (10) (2003) 8826–8836.
[136] N.A. Pansters, et al., Segregation of myoblast fusion and muscle-specific gene expression by distinct ligand-dependent inactivation of GSK-3beta, Cell. Mol. Life Sci. 68 (3) (2011) 523–535.
[137] F. Takahashi-Yanaga, T. Sasaguri, GSK-3beta regulates cyclin D1 expression: a new target for chemotherapy, Cell. Signal. 20 (4) (2008) 581–589.
[138] S. Guha, et al., Glycogen synthase kinase 3 beta positively regulates Notch signaling in vascular smooth muscle cells: role in cell proliferation and survival, Basic Res. Cardiol. 106 (5) (2011) 773–785.
[139] N. Zanou, P. Gailly, Skeletal muscle hypertrophy and regeneration: interplay between the myogenic regulatory factors (MRFs) and insulin-like growth factors (IGFs) pathways, Cell. Mol. Life Sci. 70 (21) (2013) 4117–4130.
[140] X. Wang, et al., Transient systemic mtDNA damage leads to muscle wasting by reducing the satellite cell pool, Hum. Mol. Genet. 22 (19) (2013) 3976–3986.
[141] J. Zhou, et al., GSK-3alpha is a central regulator of age-related pathologies in mice, J. Clin. Invest. 123 (4) (2013) 1821–1832.
[142] P. Cohen, M. Goedert, GSK3 inhibitors: development and their therapeutic potential, Nat. Rev. Drug Discov. 3 (2004) 479–487.
[143] H. Eldar-Finkelman, A. Martinez, GSK-3 inhibitors: preclinical and clinical focus on CNS, Front. Mol. Neurosci. 4 (2011) 32.
[144] M. Doucet, et al., Muscle atrophy and hypertrophy signaling in patients with chronic obstructive pulmonary disease, Am. J. Respir. Crit. Care Med. 176 (3) (2007) 261–269.
[145] K.J. Verhees, et al., Pharmacological inhibition of GSK-3 in a guinea pig model of LPS-induced pulmonary inflammation: II. Effects on skeletal muscle atrophy, Respir. Res. 14 (2013) 117.